Low- to high-velocity frictional properties of the clay-rich gouges from the slipping zone of the 1963 Vaiont slide, northern Italy

Fabio Ferri,[1] Giulio Di Toro,[1,2] Takehiro Hirose,[3] Raehee Han,[4] Hiroyuki Noda,[5] Toshihiko Shimamoto,[6] Marino Quaresimin,[7] and Nicola de Rossi[7]

Received 3 March 2011; revised 17 June 2011; accepted 5 July 2011; published 28 September 2011.

[1] The final slip of about 450 m at about 30 m/s of the 1963 Vaiont landslide (Italy) was preceded by >3 year long creeping phase which was localized in centimeter-thick clay-rich layers (60–70% smectites, 20–30% calcite and quartz). Here we investigate the frictional properties of the clay-rich layers under similar deformation conditions as during the landslide: 1–5 MPa normal stress, 2×10^{-7} to 1.31 m/s slip rate and displacements up to 34 m. Experiments were performed at room humidity and wet conditions with biaxial, torsion and rotary shear apparatus. The clay-rich gouge was velocity-independent to velocity-weakening in both room humidity and wet conditions. In room humidity experiments, the coefficient of friction decreased from 0.47 at $v < 5.0 \times 10^{-5}$ m/s to 0.12 at 1.31 m/s. Microstructural and mineralogical analyses of the gouge after experiments indicate that the dramatic weakening results from thermo-chemical pressurization of pore fluids (smectite decomposition to illite-type clays) and powder lubrication. In wet experiments, the coefficient of friction decreased from 0.17 at $v < 1.0 \times 10^{-4}$ m/s to 0.0 at $v > 0.70$ m/s: full lubrication results from the formation of a continuous water film in the gouge. The Vaiont landslide occurred under wet to saturated conditions. The unstable behavior of the landslide is explained by the velocity-weakening behavior of the Vaiont clay-rich gouges. The formation of a continuous film of liquid water in the slipping zone reduced the coefficient of friction to almost zero, even without invoking the activation of thermal pressurization. This explains the extraordinary high velocity achieved by the slide during the final collapse.

Citation: Ferri, F., G. Di Toro, T. Hirose, R. Han, H. Noda, T. Shimamoto, M. Quaresimin, and N. de Rossi (2011), Low- to high-velocity frictional properties of the clay-rich gouges from the slipping zone of the 1963 Vaiont slide, northern Italy, *J. Geophys. Res.*, *116*, B09208, doi:10.1029/2011JB008338.

1. Introduction

[2] On 9 October 1963 a catastrophic landslide occurred in the Vaiont Valley (Italian Southern Alps) when the northern flank of the Mount Toc slid into an artificial reservoir and generated a giant wave which destroyed the village of Longarone killing almost 2000 people. Due to the economic relevance of the site, the area was subject to three years of intense investigation and monitoring before the collapse, including the installation of benchmarks and piezometers on the slide [*Selli and Trevisan*, 1964; *Belloni and Stefani*, 1992]. It follows that the 1963 Vaiont slide represents a unique case study to unravel the processes which control the mechanics of large landslides.

[3] Most is known about the Vaiont slide: the normal stress on the sliding surface (1 to 3.5 MPa, though the pore pressure remains unknown since the four piezometers installed in the creeping mass yielded conflicting measurements), the maximum displacement (450 m), the volume of mobilized material (around 270×10^6 m^3) and, most importantly, the evolution of the mass velocity with time from the measured 3-year long creeping stage to the final collapse [*Mueller*, 1964; *Selli and Trevisan*, 1964]. The final velocity was not directly measured (the benchmarks and the monitoring system were swept away by the giant wave) but estimated to be up to 20–30 m/s [*Anderson*, 1985]. There is now general agreement that slip localized within water-saturated centimeter-thick clay-rich gouge layers (mostly made by swelling smectites) interbedded within the decimeter-thick micritic limestones [*Hendron and Patton*, 1985, 1987; *Genevois and Ghirotti*, 2005; *Veveakis et al.*, 2007]. The frictional properties of the Vaiont clay-rich gouges and

[1]Dipartimento di Geoscienze, University of Padova, Vicenza, Italy.
[2]Istituto Nazionale di Geofisica e Vulcanologia, Rome, Italy.
[3]Kochi Institute for Core Sample Research, JAMSTEC, Kochi, Japan.
[4]Korea Institute of Geoscience and Mineral Resources, Daejeon, South Korea.
[5]Seismological Laboratory, California Institute of Technology, Pasadena, California, USA.
[6]State Key Laboratory of Earthquake Dynamics, Institute of Geology, Chinese Earthquake Administration, Beijing, China.
[7]Dipartimento di Ingegneria dei Sistemi Industriali, Università degli Studi di Padova, Padua, Italy.

0148-0227/11/2011JB008338

their dependence with water content and slip rate were investigated by *Hendron and Patton* [1985] and *Tika and Hutchinson* [1999]. However, their analysis was limited in displacement (~0.24 m [*Hendron and Patton*, 1985]; ~3 m [*Tika and Hutchinson*, 1999]) and velocity (up to 16.67 μm/s [*Hendron and Patton*, 1985]; up to 0.08 m/s [*Tika and Hutchinson*, 1999]). Several authors [*Habib*, 1967; *Voight and Faust*, 1982; *Veveakis et al.*, 2007] proposed that the final acceleration and large slip rates achieved by the slide resulted from lubrication of the basal detachment due to thermal pressurization. According to this interpretation, the compaction and the temperature increase induced by shearing and frictional heating during sliding of the clay-rich layers resulted in expulsion and vaporization of the pore fluids (i.e., water). The increase in pore pressure lowered the shear strength and the dynamic friction. However, the activation of thermal pressurization was never observed in experiments or deduced from the analysis of the Vaiont samples. Another key point is the transition from the creeping stage to the final collapse which was numerically modeled [e.g., *Veveakis et al.*, 2007] but never reproduced in the laboratory.

[4] The aim of this work is to investigate the frictional properties of the clay-rich gouges at the estimated normal stress and displacements of the Vaiont slide: (1) over a wide range of slip rates (from 0.2 μm/s to 1.31 m/s), including the transition from creeping to final collapse [*Veveakis et al.*, 2007] and, (2) at different water contents (under room humidity and wet conditions). The transition toward conditions of excess water probably triggered the initial movement of the slide [*Hendron and Patton*, 1985]. To cover such large range in slip rates, we used a biaxial (low slip rates), a torsion (intermediate slip rates) and a rotary shear (high slip rates) apparatus (the range in slip rates is described in section 3).

[5] Our experimental approach will be useful to validate the models proposed to explain the final acceleration of the slide [e.g., *Vardoulakis*, 2002; *Kilburn and Petley*, 2003; *Helmstetter et al.*, 2004; *Veveakis et al.*, 2007]. The results can be extended also to seismogenic faults which are often filled, at least in their shallow (<5 km depth) sections, with clay-rich gouges [e.g., *Chester and Chester*, 1998; *Faulkner et al.*, 2003; *Hickman et al.*, 2005; *Schleicher et al.*, 2009; *Mizoguchi et al.*, 2009; *Tanikawa and Shimamoto*, 2009]. Slip rates during earthquakes are comparable to those estimated for the final stages of the Vaiont collapse (>1 m/s). It follows that weakening mechanisms similar to those activated during the slide might occur during earthquakes.

2. Geological Setting

[6] Here we briefly summarize the geology of the area. For a comprehensive review on the investigations in the Vaiont valley [see *Genevois and Ghirotti*, 2005; *Semenza and Ghirotti*, 2000]. The 9 October 1963 landslide moved on a chair-like fold with the axis plunging 9° to 20° eastward, with a flat toe (though it dips 9° to 20° eastward) and a steep back (dipping 25° to 40° north) corresponding to the northern Mount Toc flank. The latter provided the driving gravitational force for the slide (Figures 1a and 1b). The landslide slid on one or, probably, several, continuous 1 to 15 cm thick clay-rich sedimentary layers [*Hendron and Patton*, 1985] interbedded with decimeter thick micritic limestones of the Dogger-Malm Fonzaso Formation [*Cobianchi and Picotti*, 2003] (Figures 1c and 1d). The 1963 Vaiont landslide is a reactivated Holocene giant slide [*Semenza*, 1965], so in our study we will refer to the clay-rich sedimentary layers from the basal detachment as clay-rich gouges. Locally, the clay-rich layers are injected in the bounding limestones beds which might suggest fluidization and pressurization of the gouge during slip (Figure 1e). The slide displaced the Jurassic and Cretaceous rocks of the Socchér Formation (legend 3b in Figure 1b) as an almost whole block 250 m thick and ~2 km wide, corresponding to approximately 270×10^6 m^3 of rock [*Semenza*, 1965]. This is indicated by the morphology of the landslide deposit, which, though intensely fractured, preserved the pre-slide geometrical features. The block slid on average for 450 m, and it was pushed uphill for about 50 m on the opposite side of the valley.

3. Methods

3.1. Starting Material and Description of the Apparatus

[7] The samples used in our work were collected from a 5–15 cm thick clay-rich gouge layer at the hanging wall of the sliding surface of the Vaiont landslide (Figure 1d) and close to the area of provenance of the samples studied by *Hendron and Patton* [1985] (reference samples 11-3, 11-4 and 11-5) and by *Tika and Hutchinson* [1999] (reference samples 3 and 4). The gouge was disaggregated and dried in an oven at 50°C for at least 24 h to remove excess water. This temperature was low enough to avoid complete dryness of smectite surface (T > 120°C [*Morrow et al.*, 1992]) as dry conditions would be unrealistic for the Vaiont case. Before the experiments, the gouge powder was equilibrated at room humidity conditions (40–60% humidity) up to 24 h. For the low-velocity experiments, where the initial layer thickness was <1 mm, the powder was sieved at <105 μm. In intermediate- and high-velocity experiments, the initial layer thickness was 3 mm and 1 mm respectively and the gouge was not sieved. One high-velocity experiment was duplicated on the material sieved at <105 μm (experiment HVR1868 in Table 1) to investigate the effect of the comminution of large grains on the mechanical response of the gouge.

[8] X-ray powder diffraction of the starting material and quantitative analysis obtained by Rietveld refinement, revealed that the gouge is composed of 60–70% smectite, 30–40% of calcite and minor quartz. This is consistent with the analyses reported by *Hendron and Patton* [1985] and *Tika and Hutchinson* [1999] and confirms that the material tested in all the experiments is very similar in composition. Although *Hendron and Patton* [1985] report that the prevalent clay mineral is Ca-montmorillonite, in our case it was not possible to discriminate and quantify the minerals within the clay fraction, so all the swelling clays were treated as "smectites" in the refinement strategy.

[9] A wide range of slip rates was investigated, from 0.2 μm/s up to 1.31 m/s, to reproduce the velocity evolution of the landslide from the creep stage to the final collapse [see *Veveakis et al.*, 2007, Figure 6]. This required the use of three different apparatus (Figure 2): (1) a biaxial appa-

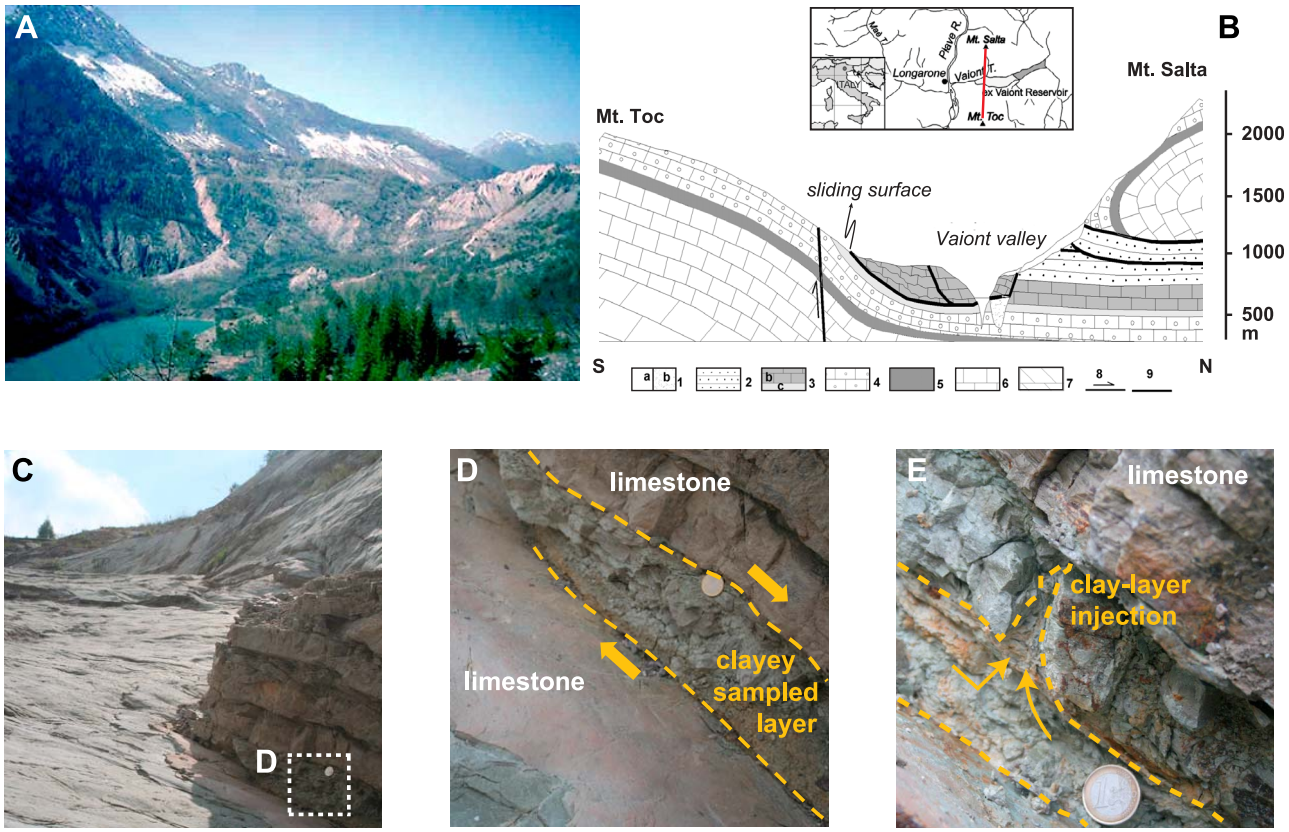

Figure 1. (a) Panoramic view of the Vaiont landslide from NE (original photograph by E. Bromhead). (b) N-S geological section from the Monte Toc to the Monte Salta before 9 October 1963 (modified after *Semenza and Ghirotti* [2000]). Legend: 1, a Quaternary; b stratified alluvial gravels; 2, Scaglia Rossa Fm. (Upper Cretaceous–lower Paleocene); 3, Cretaceous-Jurassic Formations. (Socchér Formation sensu lato and coeval): b, Socchér Formation sensu stricto, and c, Ammonitico Rosso and Fonzaso Formations; 4, Calcare del Vaiont Formation (Dogger); 5, Igne Formation (Upper Liassic); 6, Soverzene Formation (Lower and Middle Liassic); 7, Dolomia Principale (Upper Triassic); 8, faults and overthrusts; 9, failure surfaces of the landslide with chair-like geometry. (c) Detail of the sliding surface. (d) Clay-rich layer in contact with the sliding plane sampled for the experimental investigation. (e) Clay layer injected in the upper bounding limestones.

ratus at the University of Hiroshima (Hiroshima, Japan) for the low-velocity friction (LVF) experiments (from 0.2 to 100 μm/s: LVF experiments, Figure 2a), (2) a compression-torsion MTS809 fatigue testing machine at the Department of Engineering, University of Padova (Vicenza, Italy) for intermediate-velocity (IVF) experiments (from 0.050 mm/s to 50 mm/s: IVF experiments, Figure 2b) and (3) a high-velocity friction (HVF) rotary machine at the Kochi Core Center (Kochi, Japan) for high-velocity experiments (from 0.01 to 1.31 m/s: HVF experiments, Figure 2c). The complete list of the experiments is reported in Table 1.

[10] The experiments were performed at room humidity and wet conditions. Wet conditions were obtained by capillarity or by adding distilled water to the gouge powder (see details in sections 3.2 and 3.4). Complete water saturation during the experiment was probably not obtained since (1) air might have been trapped within the pores and (2) water was not fluxed throughout the gouge.

3.2. Low-Velocity Friction Experiments

[11] Biaxial experiments were performed in the range 0.2 μm/s to 100 μm/s by placing about 1.5 g of the gouge between blocks of gabbro in a double direct shear configuration at constant normal stress σ_n (Figure 2a). The thickness of the gouge was 0.5–1.0 mm, the area of the sliding surface 40 mm × 50 mm and the maximum displacement 20 mm. The sliding surfaces of the gabbro blocks were polished with SiC 80# to impose an initial roughness to impede slip localization at the gouge/wall rock boundary [*Niemeijer and Spiers*, 2006]. We applied a normal load to the blocks corresponding to 5 MPa and then sheared the gouge by pushing the inner block. To easily achieve steady state conditions, the samples were pre-compacted at a pressure slightly higher than the target one and kept under overpressure for 12–24 h before the experiment. For wet experiments, the gabbro-gouge-gabbro sandwich was clamped after pre-compaction and immersed for several hours into 1 cm deep

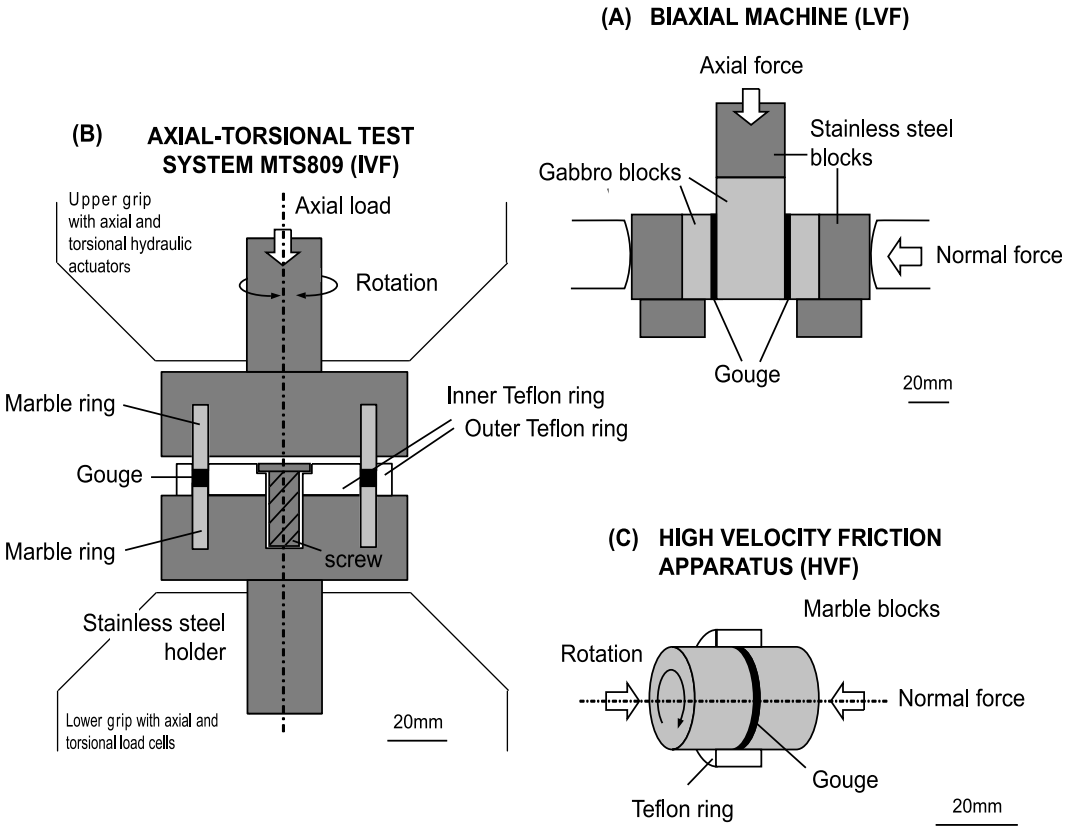

Figure 2. Schematic diagrams of the apparatus used for the friction tests in the three different velocity ranges. (a) Biaxial machine for low-velocity friction experiments (LVF). (b) Axial-torsional test system MTS809 for intermediate-velocity friction experiments (IVF). (c) High-velocity friction apparatus for high-velocity friction experiments (HVF). In every scheme the location of the gouge and the direction of the normal stress and shear stress (simple shear in Figure 2a, rotary shear in Figures 2b and 2c) are reported.

distilled water bath so that partial to total saturation was achieved through capillarity. In long duration experiments, water was sprinkled from a flask directly onto the sample to prevent sample dryness along the outer rims of the assembly.

[12] We performed velocity-stepping tests with fast speed change obtained by electromagnetic clutches. Details of the biaxial apparatus are given by *Noda and Shimamoto* [2009]. Two different procedures were adopted: in experiments HTB27 and HTB28 (Figure 3a) and HTB26 (Figure 3b) velocity was changed after a fixed displacement of 2–3 mm even if steady state was not reached. For example, the velocity sequence of run HTB28 was 16.96 → 32.90 → 16.96 → 1.01 → 16.96 → 32.90 → 16.96 → 1.01 μm/s. In experiment HTB24 and HTB25 (Figure 3b), a velocity v_1 was imposed to the inner block and kept constant until the steady state friction μ_{1ss} was reached. After that, velocity was changed to v_2 until μ_{2ss} was achieved, and so on for every velocity step.

3.3. Intermediate-Velocity Friction Experiments

[13] Experiments at intermediate velocity were performed with the MTS809, an hydraulic axial-torsional test system. The machine has a vertical arrangement with a stationary grip to the lower side and a hydraulic grip to the upper side which applies the axial load and the rotary movement (Figure 2b). A pair of load cells measures the normal load and the torque during the test, while the Linear Variable Displacement Transducer (LVDT) and the Angular Displacement Transducer (ADT) measure the axial (= vertical) displacement and the angular position respectively. The main technical characteristics of the system are the following: (1) axial load, 100/10 kN (double full scale calibration), (2) torsional capacity, 1100/100 N m (double full scale calibration), and (3) displacement sensor, LVDT ± 100 mm, ±10 mm (double full scale calibration), and angular sensor, ADT ± 90°, ±5° (double full scale calibration). The sample assembly was modified to investigate powder material: the gouge was placed between two Carrara marble hollow cylinders with 50/60 mm internal/external diameter. Two Teflon® rings (outer and inner) were used to confine the gouge and prevent its leakage during the run. The surfaces of the marble cylinder at the contact with the gouge were ground with SiC 80# to reduce slip localization at the gouge/wall rock boundary. About 3–4 g of powder were loaded for every experiment: this mass corresponded to an average initial thickness of ~3 mm. The two marble hollow cylinders were glued onto the steel made sample holders. Given the hollow shape of the sandwiching wall rocks, slip rate v, slip d and τ in the gouge increase with sample radius, with r_1 is

Table 1. Run Table of the Experiments Performed on the Vaiont Clay-Rich Gouges[a]

Run	σ_n (MPa)	v (m/s)	V_{H2O} (mL)	D (mm)	D_c (mm)	μ_p	μ_{ss}	SD
Low-Velocity Experiments: Biaxial Apparatus								
HTB24	5	1.01E-06	capillarity	18.6			0.16	(0.00)
		1.01E-04					0.18	(0.00)
HTB25	5	5.03E-07	capillarity	19.2			0.17	(0.00)
		5.03E-05					0.16	(0.00)
HTB26	5	1.90E-07	capillarity	8.3			0.17	(0.00)
		1.79E-06					0.16	(0.01)
		1.77E-05					0.14	(0.00)
HTB27	5	1.90E-07	RH	8.0			0.46	(0.00)
		1.79E-06					0.46	(0.00)
		1.77E-05					0.45	(0.00)
HTB28	5	1.01E-06	RH	19.1			0.43	(0.00)
		1.70E-05					0.42	(0.00)
		3.29E-05					0.43	(0.00)
Intermediate-Velocity Experiments: Rotary Torsion MTS809								
v1	1	5.00E-05	RH	10.0	3.75	0.50	0.42	(0.00)
v2	1	5.00E-05	RH	10.0	1.78	0.45	0.43	(0.00)
v3	1	5.00E-05	RH	10.0	2.17	0.44	0.43	(0.00)
v4	1	5.00E-05	RH	6.0	1.37	0.44	0.43	(0.00)
		5.00E-04		33.6			0.49	(0.00)
v5	1	5.00E-05	RH	6.0	2.79	0.48	0.44	(0.00)
		1.00E-03		33.6			0.52	(0.00)
v6	1	5.00E-05	RH	6.0	1.58	0.48	0.47	(0.00)
		5.00E-03		33.6			0.56	(0.01)
v7	1	5.00E-05	RH	6.0	1.75	0.47	0.46	(0.01)
		0.05		33.6			0.65	(0.01)
High-Velocity Experiments: High-Velocity Friction Apparatus[b]								
1355	1	1.31	0.4	16.95	17.00	0.19	0.05	(0.01)
1377	1	1.31	0.4	35.87	27.50	0.10	0.01	(0.01)
1388	1	1.31	0.4	26.34	19.10	0.17	0.01	(0.01)
1356	1	0.70	0.4	17.40	16.50	0.07	0.02	(0.01)
1378	1	0.70	0.4	27.89	20.00	0.07	0.02	(0.02)
1357	1	0.17	0.4	18.90	5.00	0.23	0.11	(0.00)
1379	1	0.17	0.4	5.10		0.13	0.11	(0.01)
1389	1	0.17	0.4	31.07	3.00	0.08	0.00	(0.00)
1358	1	0.04	0.4	10.81		0.03	0.02	(0.00)
1380	1	0.04	0.4	7.31	0.06	0.16	0.03	(0.01)
1359	1	0.01	0.4	5.92	0.03	0.05	0.03	(0.01)
1381	1	0.01	0.4	1.03	0.06	0.03	0.00	(0.01)
1372	1	1.31	RH	34.57	8.99	0.71	0.14	(0.01)
1868[c]	1	1.31	RH	29.53	7.50	0.73	0.09	(0.01)
1373	1	0.70	RH	34.29	8.70	0.62	0.16	(0.02)
1374	1	0.17	RH	10.68	9.50	0.74	0.50	(0.04)
1702	1	0.17	RH	10.49		0.76	0.42	(0.02)
1375	1	0.04	RH	10.19			0.79	(0.02)
1709	1	0.04	RH	10.50			0.74	(0.01)
1710	1	0.04	RH	6.79			0.71	(0.01)
1376	1	0.01	RH	7.28			0.77	(0.02)

[a]Parameters are σ_n = normal stress; v = slip rate; V_{H2O} = volume of H_2O; RH = room humidity; D = displacement; D_c = critical slip distance; μ_p = peak friction coefficient; μ_{ss} = steady state friction coefficient; SD = standard deviation for μ_{ss}.

[b]μ Teflon = 0.06.

[c]Gouge sieved at <105 mm.

outer diameter and r_2 is the inner diameter and R is the revolution rate imposed by the motor. We determined the slip rate for the gouge as the "equivalent slip rate" v_e [*Shimamoto and Tsutsumi*, 1994; *Hirose and Shimamoto*, 2005]:

$$v_e = \frac{4\pi R\left(r_1^2 + r_1 r_2 + r_2^2\right)}{3(r_1 + r_2)}. \quad (1)$$

As a consequence, displacement d is

$$d = v_e t. \quad (2)$$

Experiments were performed at sliding equivalent velocity ranging from 0.050 mm/s to 50 mm/s under a constant normal stress of 1 MPa (Table 1). All experiments were carried out as follows: (1) a preliminary step where an axial compression load ramp was applied up to 1 MPa over the sample surface; this stress was maintained during the next steps; (2) a frictional loading step at low slip rate (v_e = 0.050 mm/s): during this step, friction increased with slip to a constant value of about 0.45 (Figure 5); and (3) a high-speed step with different target slip rates (ranging from 0.050 to 50 mm/s) (Figure 5).

[14] The displacement during the high-speed step varied with the imposed slip rate: at 0.050 mm/s total slip was 10 mm while at velocity >0.050 mm/s, total slip was 33.6 mm. Due to technical difficulties, IVF experiments were performed only at room humidity conditions.

3.4. High-Velocity Friction Experiments

[15] Experiments were performed in the high-speed rotary shear testing apparatus of *Shimamoto and Tsutsumi* [1994] (further details are given by *Tanikawa and Shimamoto* [2009]). The sample assembly is schematically reported in Figure 2c and consists of two Carrara marble cylinders with 24.95 mm diameter and 20 mm length sandwiching the gouge. One gram of gouge was placed between two marble cylinders to produce a 0.5–1.0 mm thick layer. The surfaces of the marble in contact with the gouge were grinded with 80# mesh SiC powder to reduce slip localization at the gouge/wall rock boundary. The cylinders were forced into a Teflon® sleeve which acted as confining medium during the rotation of the sample. In wet experiments, 0.4 ml of distilled H_2O was added to the powder immediately before the experiment. Experiments were performed at rotation speeds ranging from 7 to 1500 rpm corresponding to 0.01 m/s and 1.31 m/s equivalent velocity (equation (1)) with displacement up to ~36 m (Table 1). Experiments were repeated to check for reproducibility and run HVR1868 was performed at 1.31 m/s on the gouge sieved at <105 μm.

4. Results

4.1. Mechanical Data

4.1.1. Friction in Low-Velocity Experiments

[16] The evolution of the friction coefficient versus displacement is reported in Figure 3 for representative experiments performed at room humidity (Figure 3a) and wet (Figure 3b) conditions. The friction coefficient μ is calculated as the ratio between the shear stress τ and the normal stress σ_n. Hereafter we will denote μ_p as the peak friction and the μ_{ss} as the steady state friction (Table 1).

[17] At room humidity, the steady state friction coefficient μ_{ss} ranges from 0.42 to 0.46 (Figure 3a) and stick slip is observed in experiments HTB27 and HTB28 (Figure 3a) where the amplitude of the friction oscillations observed at constant velocity increases when velocity decreases.

[18] At wet conditions, μ_{ss} is generally achieved after 2 to 5 mm of slip and ranges from 0.14 to 0.18 (Figure 3b). At every velocity change, a peak in the friction behavior is

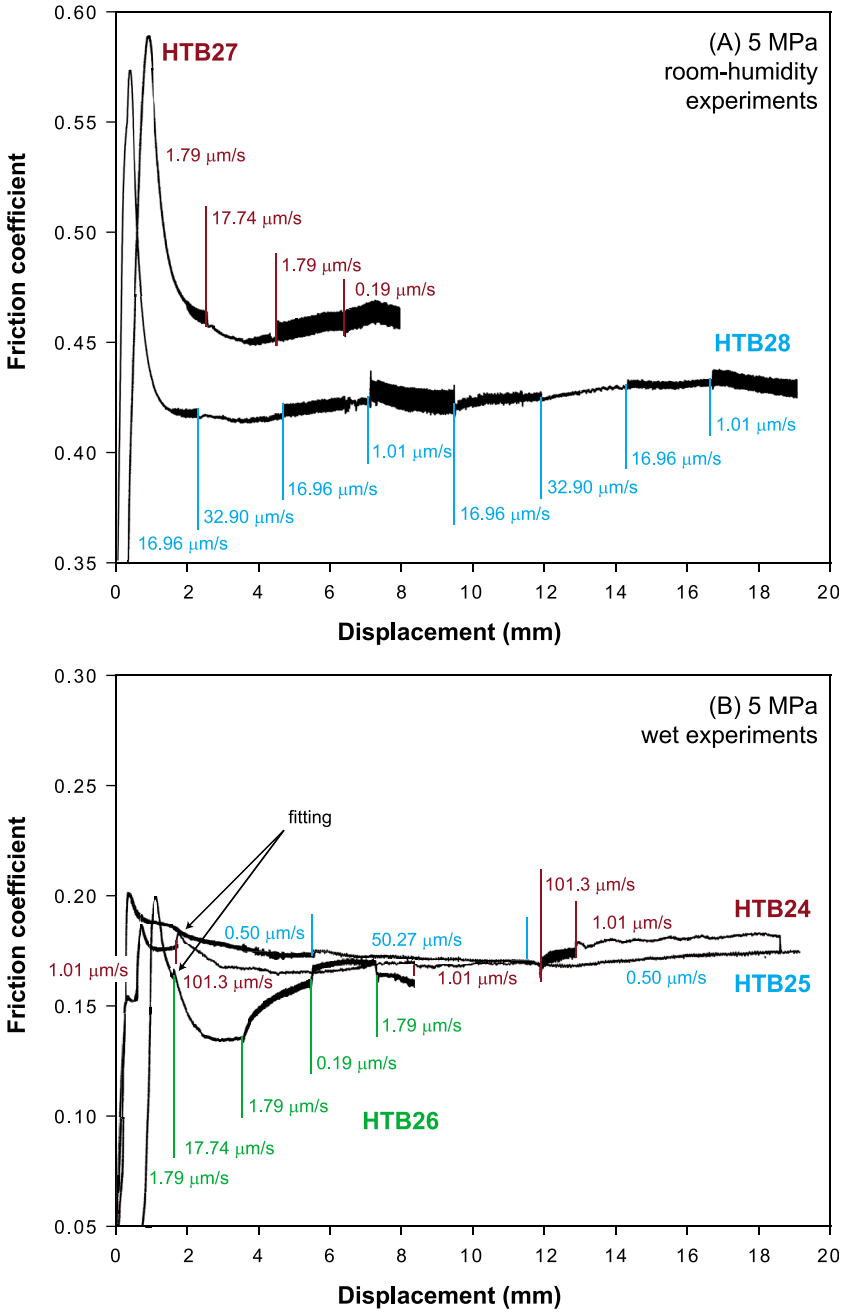

Figure 3. Friction coefficient versus displacement in representative biaxial experiments at 5 MPa normal stress: (a) HTB27 and HTB28, room humidity conditions and (b) HTB24, HTB25 and HTB26, wet conditions. Velocity steps are reported. The two peaks (direct effect) in HTB24 and HTB26 are fitted in Figure 4 to obtain the rate- and state-dependent parameters (see text for details).

observed which reflects the velocity dependence of the friction coefficient. Most peaks have irregular shape and are not well defined, excepting the initial peaks observed in experiments HTB24 and HTB26 after 2 mm displacement (Figure 3b). For these experiments, the rate and state dependent frictional constitutive laws [*Dieterich*, 1979; *Ruina*, 1983] were used to describe the mechanical response of the slipping zone at changing slip rate (Figure 4). The slip rate dependence of the steady state friction is given by the difference (a–b), where "a" is the direct effect and "b" is the evolution effect. For an increase in velocity, if (a–b) < 0, the behavior is velocity-weakening and the system is intrinsically unstable; if (a–b) > 0, the behavior is velocity-strengthening and the system intrinsically stable [e.g., *Marone*, 1998]. The constitutive parameters of the rate and state friction law were obtained by fitting the experimental data for the velocity step from 1.01 μm/s to 101.3 μm/s in HTB24, and from 1.79 μm/s to 17.74 μm/s in HTB26 with the slip law [*Ruina*, 1983] and the aging law [*Dieterich*, 1979] (Figures 3 and 4). The fit by means of the slip and aging laws are comparable, respectively (a–b) = -4.56×10^{-3} and -4.62×10^{-3} for HTB24, and -7.42×10^{-3} and

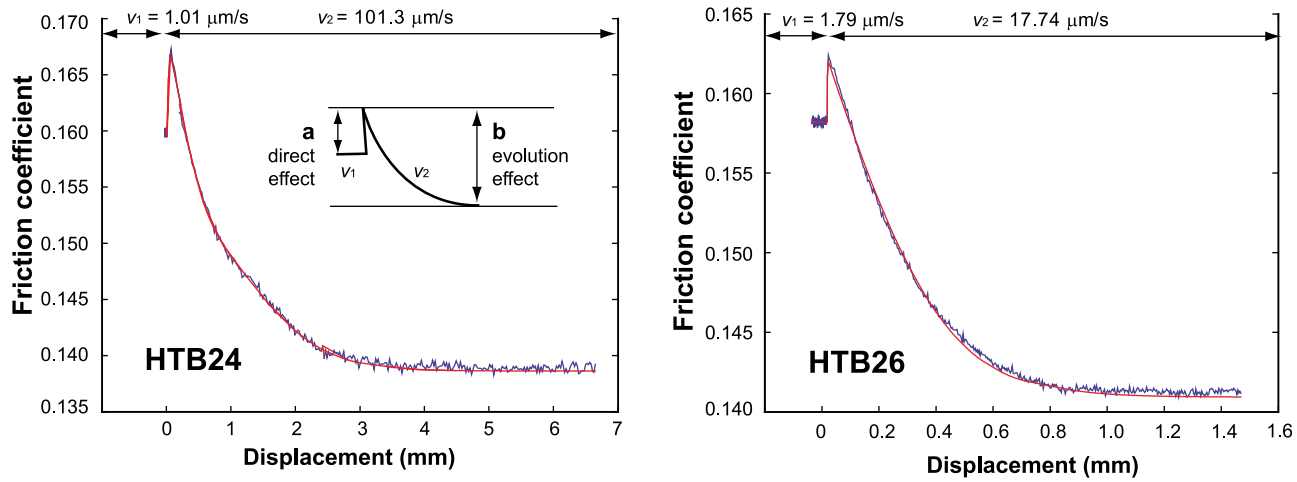

Figure 4. Results of the fitting procedure with the aging law (reported as a red line) for the two velocity steps imposed in wet experiments HTB24 and HTB26. The red curve describes the rate- and state-friction law.

-7.64×10^{-3} for HTB26. It follows that in this velocity range, wet smectite-rich gouges from the Vaiont slide basal detachment are velocity weakening. In HTB25, friction was almost velocity independent with steady state values of 0.16–0.17.

4.1.2. Friction in Intermediate-Velocity Experiments

[19] In intermediate-velocity experiments, the Teflon® rings used to confine the gouge exerted a frictional resistance which was not negligible [e.g., *Kitajima et al.*, 2010]. The contributions of Teflon® ring to friction was determined by a calibration test without gouge and without achieving contact between the rock cylinders. The torque value was measured as a function of the rotation angle and subtracted. The corrected values of friction coefficients μ_{ss} and μ_p are reported in Table 1 and Figure 5.

[20] At room humidity, the average friction is 0.43 at 0.050 mm/s and increases to 0.65 at 50 mm/s (Figure 5). The increase in the friction coefficient with slip rates denotes a velocity strengthening behavior. In the "frictional loading step" performed at 0.050 mm/s (which always preceded the high-velocity step), the friction coefficient progressively increased from 0.42 to ~0.47 in successive

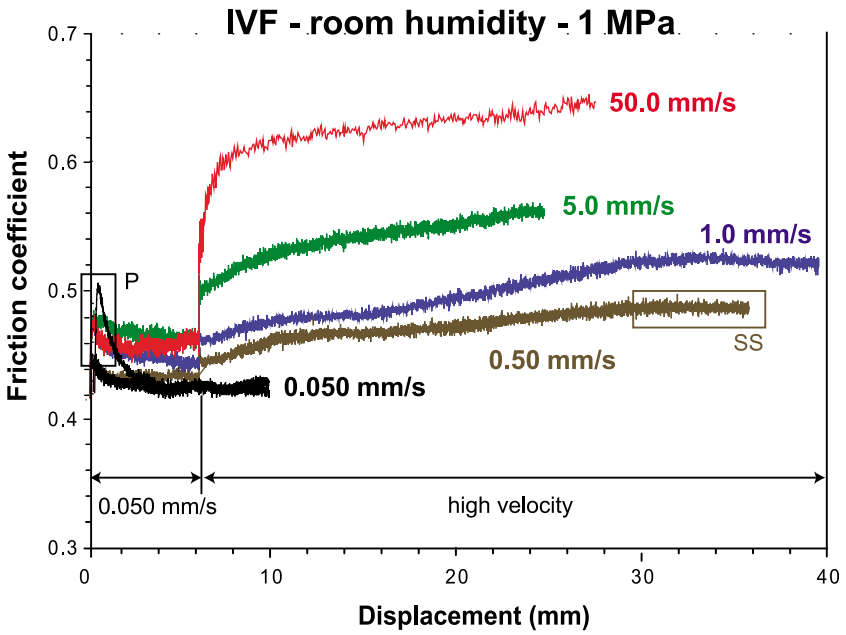

Figure 5. Friction coefficient versus displacement in room humidity experiments performed in the axial-torsional test system MTS809. Each experiment consists in two steps: (1) an initial low velocity step at 0.050 mm/s for ~6 mm followed by (2) an abrupt increase in velocity for 33.6 mm of displacement. The box P indicates the peak friction coefficient at 0.050 mm/s, the box SS indicates the steady state value during the high-velocity step.

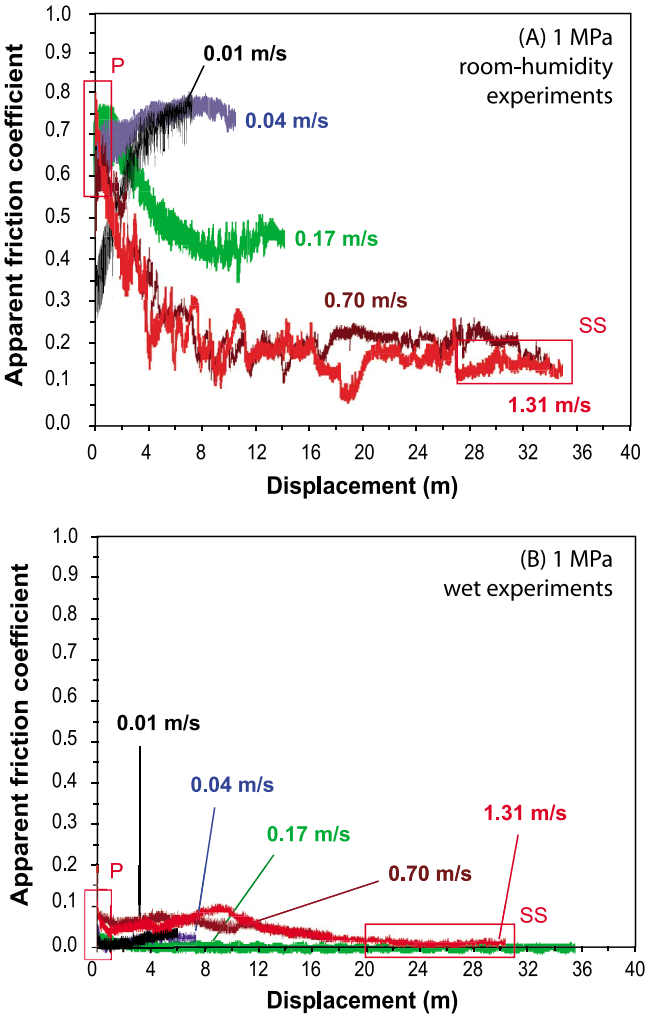

Figure 6. Apparent friction coefficient as function of displacement in experiments performed in high-velocity friction apparatus at 1 MPa and velocity ranging from 0.01 to 1.31 m/s. The apparent friction coefficient decays from initial peak (indicated by the box P) to steady state value (indicated by the box SS). (a) At room humidity the steady state friction decreases with increasing velocity (velocity weakening). (b) Under wet conditions the difference between peak and steady state value is <0.10 and the steady state friction is between zero (full lubrication) and 0.10.

runs (v1 to v7 in Table 1). This can be interpreted as due to the development of a fabric within the gouge as due to grain rotation and alignment. In fact, the starting material was loaded once at the beginning of the tests and sheared at progressively increasing velocities. Nevertheless, these values for the friction coefficient are of the same order as those obtained with the biaxial apparatus at similar slip rates (Figure 3a).

4.1.3. Friction in High-Velocity Experiments

[21] At high velocity, the behavior of friction with slip for the clay-rich gouge under room humidity (Figure 6a) and under wet (Figure 6b) conditions is remarkably different. In Figure 6 the friction coefficient is reported as "apparent friction coefficient" because the pore pressure within the gouge could not be monitored. Changes in pore fluid pressure are particularly relevant in high-velocity experiments where thermomechanical reactions and water expulsion by dynamic compaction of the gouge layer take place (see Par. 4.2). We reported the experimental data in Table 1, including the slip weakening distance D_c [e.g., *Cocco et al.*, 2009] which is defined as the amount of slip required to reduce $\mu_p - \mu_{ss}$ by 95% [*Mizoguchi et al.*, 2009]. The data for μ_p and μ_{ss} were corrected for Teflon® friction. The Teflon® rings used to confine the gouge exerted a frictional resistance which was taken into account especially for wet experiment where the value of steady state friction was extremely low. Teflon® friction was determined by *Mizoguchi et al.* [2007] to be about 0.10, but in wet experiments HVR1389 and HVR1381, steady state friction was as low as 0.06 before applying the correction for Teflon® friction. So we subtracted a value of 0.06 in all the experiments: this dynamic friction coefficient for Teflon® is consistent with the value reported by *Makinson and Tabor* [1964].

[22] At room humidity conditions, the dependence of friction with slip and slip rate is complex. At slip rates ranging from 0.01 and 0.04 m/s, no peak friction is observed and friction increases to ~0.71–0.79 after 4–5 m displacement. At velocity of 0.17 m/s, friction decreases with increasing slip from an initial peak of 0.76 to 0.4–0.5. A more dramatic friction decrease occurs at slip rates of 0.70 and 1.31 m/s, where $\mu_p = 0.62–0.73$ and $\mu_{ss} = 0.09–0.16$ are achieved after 7–9 m displacement. In particular, at velocities of 0.70 and 1.31 m/s and under room humidity conditions, the reduction of friction with slip occurs with dilatancy of the slipping zone. In Figure 7 we report (1) the shear stress τ, (2) the normal load σ_n, and (3) the axial displacement ε (or the movement of the horizontal piston) as a function of slip for two experiments performed at 1.31 m/s at room humidity conditions: HVR1372 (not sieved gouge) and HVR1868 (gouge sieved at <105 μm). An increase in ε corresponds to dilatancy of the slipping zone and a decrease in ε corresponds to shortening. The two experiments are remarkably similar despite the different grain size of the starting materials. In the initial 1.5 m of slip, the slipping zone shortens by about 100 μm due to compaction of the grains. From ~3.5 m to 18 m in HVR1372 and to 22 m in HVR1868, the gouge zone dilates of 200 and 280 μm respectively, with several pulses of dilation and shortening (the largest one of 200 μm in HVR1372 between 4 and 6 m). During the final slip, from 18 to 34 m in HVR1372 and from 22 to 30 m in HVR1868, the slipping zone shortens without visible gouge loss from the Teflon® sleeve. During the experiment, the normal stress measured at the load cell oscillates between 1.0 and 1.15 MPa. There are systematic relationships between ε and σ_n during the transient toward the steady state shear stress, with σ_n increasing when the sample dilates and decreasing when the sample shortens. The behavior of the shear stress τ is more complex and can decrease or increase with dilatancy.

[23] At wet conditions, the frictional value evolves smoothly from peak- to steady state conditions with increasing slip so that the steady state conditions are achieved after about 4 m slip at $v < 0.17$ m/s and more than 16 m at $v > 0.70$ m/s. μ_{ss} is between 0.05 and 0.0 (full

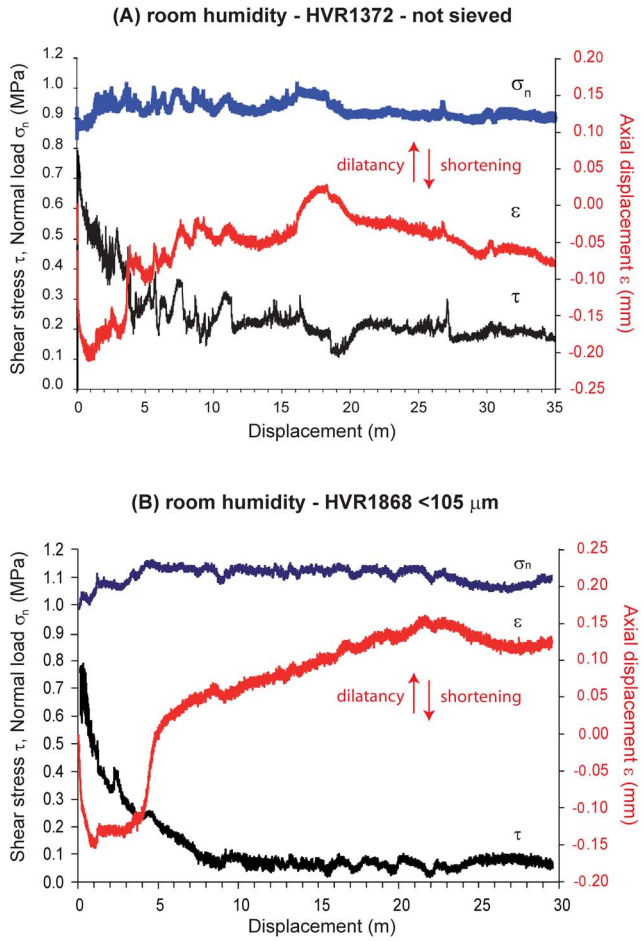

Figure 7. Normal load σ_n, axial displacement ε and shear stress τ in room humidity experiments HVR1372 (not sieved gouge) and HVR1868 (gouge sieved at <105 μm) as a function of displacement (see text for details). Dilatancy of the sample (increase of ε) is observed after ~3.5–4.5 m displacement, concomitant to the increment of σ_n and decrement of τ. Shortening (decrease of ε) occurs above ~18–22 m of displacement.

lubrication) excepting HVR1357 and HVR1379 at 0.17 m/s where μ_{ss} = 0.11. The difference μ_p - μ_{ss} is always <0.16.

4.2. Mineralogical Data

[24] After the experiments, the gouge material was extracted, disaggregated and analyzed by X-ray Powder Diffraction at the University of Padova. We selected two high-velocity experiments at 1.31 m/s, HVR1388 for wet conditions and HVR1868 for room humidity conditions. Since velocity increased as a function of the distance from the center of the cylinder (where v = 0), we hand-collected the powder from the rim portion of the slip zone where the velocity and the temperatures achieved are expected to be maximum [*Mizoguchi et al.*, 2009; *Kitajima et al.*, 2010]. Experiment HVR1868 was similar to HVR1373 (0.70 m/s) and HVR1372 (1.31 m/s) since the gouge drastically changed in color from the starting green-yellowish powder into a dark brown-black one after deformation. Moreover, only in the case of the room humidity experiments (HVR1868, HVR1373 and HVR1372) the Teflon® rings evidenced an embayment (black in color) on the inner side at the contact with the gouge, which was interpreted as effect of Teflon® decomposition due to frictional heating.

[25] In Figure 8 comparison of the XRPD spectrum of the staring material (Figure 8a) with HVR1388 (Figure 8b) and HVR1868 (Figure 8c) shows that (1) at wet conditions, even for slip rates of 1.31 m/s, no mineralogical variation occurs, and the diffraction pattern shows the characteristic broad peak of smectite at $2\theta \approx 8°$ and (2) at room humidity conditions, for slip rates of 1.31 m/s, smectite is substituted by an illite-type clay and fluorite is present. The collapse of the smectite to an illite-type structure results from the temperature increase within the slipping zone with consequent expulsion of interlayer water molecules. This type of dehydration occurs at 1 MPa confining pressure in the temperature interval 100–200°C [*Brindley and Brown*, 1980, p. 213] depending on the type of exchangeable cation (Na^+, Ca^{2+}, etc.) and on the structure of smectite. The structural collapse presumably does not affect the chemical composition of cations in interlayers (e.g., Ca^{2+} and Na^+), so the term "illite-type" does not refer to illite in the strictest sense (i.e., with K^+ in interlayers). The decomposition of Teflon® occurs above 260°C (http://www2.dupont.com/Teflon_Industrial/en_US/products/selection_guides/properties.html) with the release of fluorine gas which presumably reacted with calcite of the gouge to produce fluorite. These observations suggest that under room humidity conditions, temperature increased at least up to 260°C at the outer margin of the cylinder (i.e., at the contact with the Teflon®) and that the temperature increase propagated toward the center of the gouge layer with time and displacement. [*Mizoguchi et al.*, 2009; *Kitajima et al.*, 2010].

4.3. Microstructural Observations

[26] Figure 9 reports scanning electron microscope backscattered (SEM-BS) images from experiments performed at room humidity (Figures 9a–9e) and wet (Figures 9f–9j) conditions. In LVF experiments (HTB25 in Figure 9g) the thin sections were cut from the central part of the blocks where the influence of the side effects (e.g., absence of lateral confinement) was less pronounced. For HVF experiments (performed in the rotary shear apparatus, Figures 9b, 9c, 9d, 9e, 9h, 9i and 9j), the slip velocity increased with sample radius and thin sections were cut tangential to the outer rims of the sample assembly where the slip velocity was maximum and close to the set value. The sense of shear is left lateral and pictures are oriented with the rotating cylinder to the left side. To prevent clay swelling during sample preparation and to preserve the original microstructures, no water was used and thin sections were dry cut and hand-polished with diamond paste (DP paste 1 μm, Struers) diluted with petroleum ether (Sigma-Aldrich n.320447).

[27] The microstructure of the gouge at room humidity and wet conditions are different both at the initiation and at the end of sliding. At room humidity conditions, the starting material is a grain-supported matrix made of angular clasts of calcite, quartz and clay aggregates (Figure 9a; for HVR1868, the initial grain size was <105 μm). The texture evolves with increasing sliding velocity due to comminu-

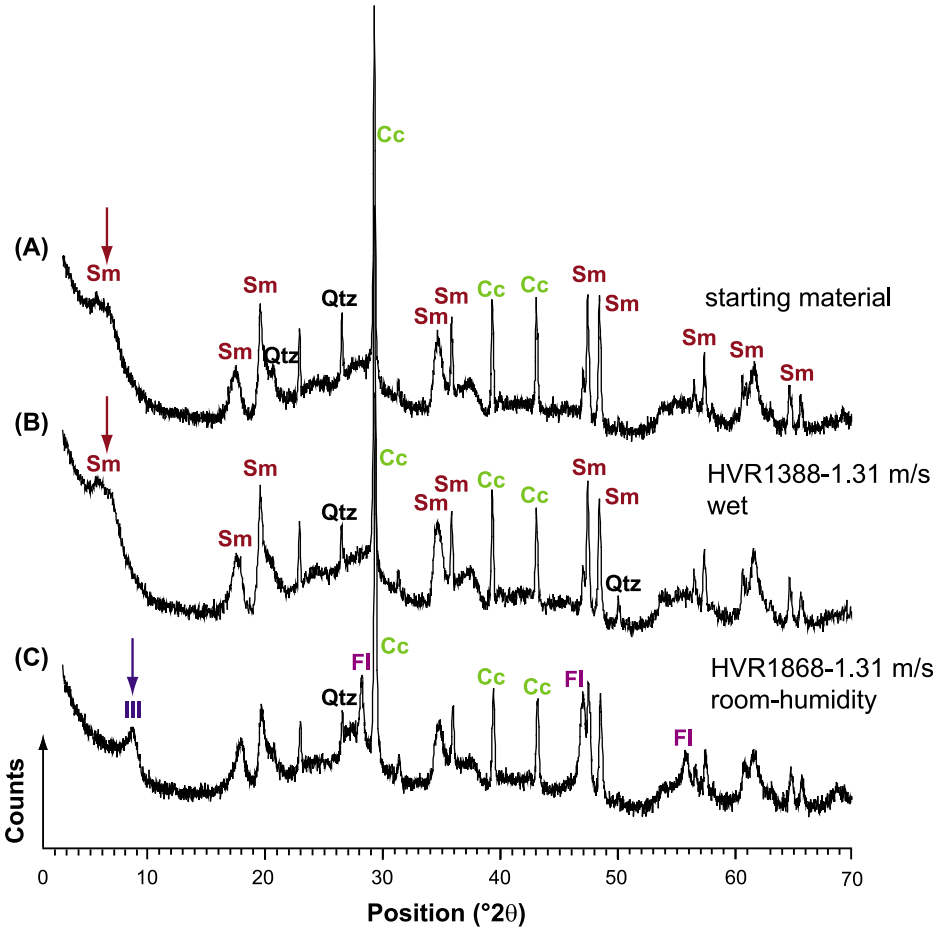

Figure 8. X-ray powder diffraction (XRPD) analysis results. In the ordinates, the maximum counts per second are 3600. Abbreviations are Qtz = quartz, Cc = calcite; Sm = smectite; Ill = illite-type clay; Fl = fluorite. XRPD analysis (a) of the starting gouge and (b) of the gouge layer after the water-saturated experiment (HVR1388, v = 1.31 m/s). The mineralogy of the two gouges is identical; the arrow indicates the broad peak at low diffraction angle characteristic of smectite (Sm). (c) XRPD analysis of the gouge layer after the room humidity experiment (HVR1868, v = 1.31 m/s). The spectrum has the peaks of fluorite (Fl) and the arrow indicates the typical peak of the illite-type clay (Ill) at low diffraction angle.

tion, decomposition and grain rolling. At 0.01 m/s the grain size reduces from the stationary side toward the contact with the rotational side (left in Figure 9b), where a fine grained ~150 μm thick layer is present. At 0.04 m/s the grain size reduction affects most of the gouge layer although some angular clasts up to 300 μm survive and R-type shears develop at the contact with the rotational side (Figure 9c). At 0.70 and 1.31 m/s (Figures 9d and 9e) a granular layer made of comminuted grains and clay clast aggregates CCAs [*Boutareaud et al.*, 2008] is present. CCAs have calcite, quartz and clay aggregates nuclei rimmed by ultrafine-grained particles distributed in concentric layers. In HVR1373 (Figure 9d), the CCAs can be up to 100 μm diameter with fine-grained concentric layer up to 50 μm thickness. At the contact with the rotational side, a 70 μm fine grained layer develop which is cut by R-and Y-type shears. At 1.31 m/s (experiment HVR1372, Figure 9e), the fine grained layer at the contact with the marble cylinder is less thick (~50 μm) and more homogeneous. The average dimension of CCAs is smaller (around 50 μm) and the cortex thinner (<20 μm) with respect to CCAs from HVR1373. The same textures found in HVR1372 were obtained in experiment HVR1868 (not reported in Figure 9), which was also performed at 1.31 m/s but on a gouge sieved at <105 μm.

[28] At wet conditions, the starting material is a gouge with a smectite-supported matrix wrapping (1) calcite and quartz grains up to ~500 μm in size (Figure 9f) and (2) elongated aggregates of clay + crystal fragments with dimensions from tens to hundreds of micrometers. The microstructure of the slipping zone does not significantly vary with increasing velocity, in fact, (1) the average dimensions and shape of the grains is velocity independent (compare Figure 9h with Figure 9i) and (2) the aggregates of clay + crystal fragments are preserved up to ~0.70 m/s sliding velocity (as evidenced by dessication cracks developed parallel or normal to the long axes, Figures 9g–9i), (3) Y- and P-shears are found only in the experiments at v = 1.31 m/s (Figure 9j). The above microstructures and the very low friction measured at v > 0.01 m/s suggest that sliding occurred on the water layers adsorbed at the surface of clay

particles and, once the clay-rich gouge was compacted and water progressively expelled, along a continuous water film formed at the clay-gouge/wall rock boundary (D. A. Lockner, personal communication, 2010, to G. Di Toro). In experiment HVR1388 performed at a slip rate of 1.31 m/s, two 10–20 μm thick ultrafine layers are present at the gouge-wall rock contact (Figure 9j). P-type shears develop from the rotational side to the middle part of the gouge, where Y-type shears are observed together with preserved large grains of calcite and quartz (about 50–100 μm in size).

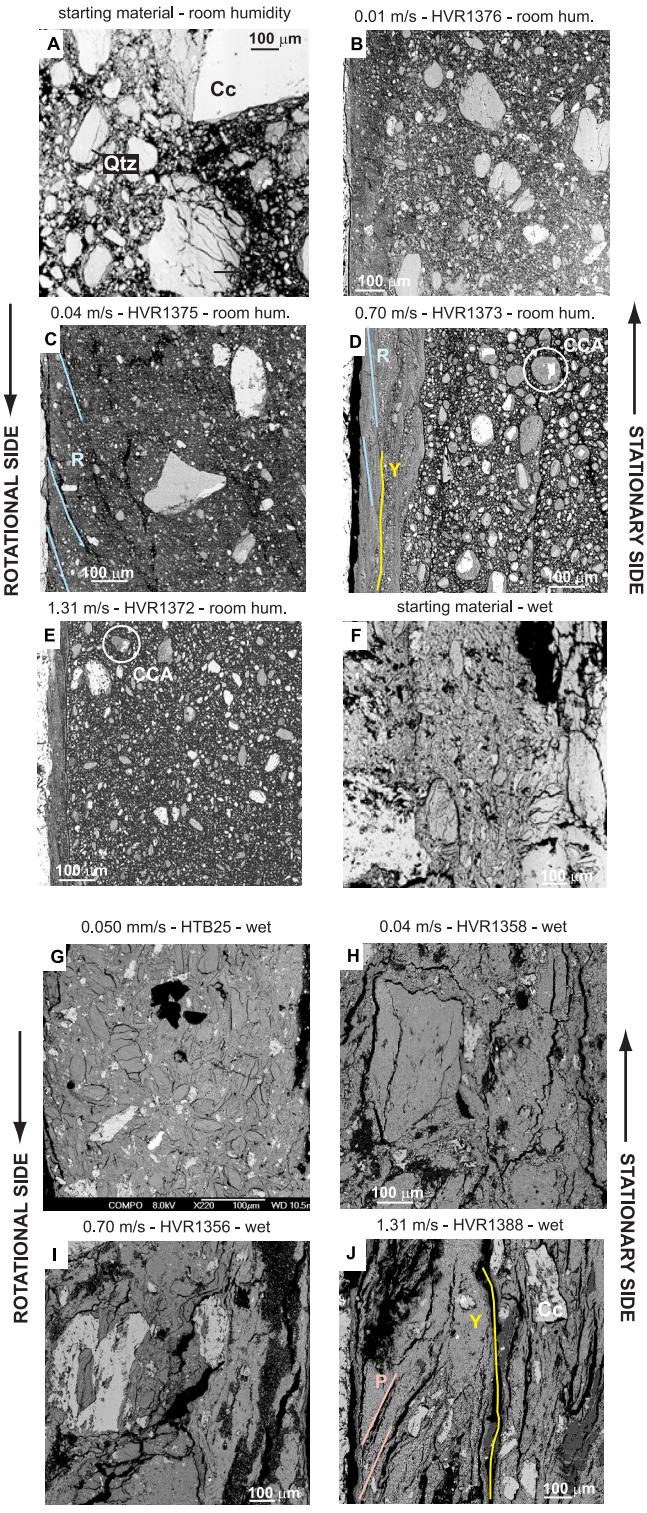

5. Discussion

5.1. Interpretation of the Experimental Data

[29] The results of our experimental work are summarized in Figure 10 where the steady state friction coefficients for room humidity and wet experiments are reported as a function of slip rate. The friction coefficient of the Vaiont clay-rich gouges evolves with increasing velocity and water content, suggesting the activation of different weakening (and strengthening in the case of room humidity experiments) mechanisms. To interpret these mechanisms, we will first estimate the temperature evolution of the slipping zone by means of a simple thermal analytical model, combined with constraints from the mineralogical and microstructural observations. The temperature increase triggers mineral reactions (e.g., H_2O release due to decomposition of smectite to an illite-type clay) and changes in the surface properties of minerals (e.g., removal of moisture from the surface of clay particles). Since the instability of the Vaiont landslide most probably took place in the water-saturated regime [*Hendron and Patton*, 1985], only the frictional properties of the gouge at wet conditions will be extrapolated and compared to the mechanical data of the landslide.

5.1.1. Estimate of the Temperature Increase During Sliding

[30] Though we did not measure the temperature during the experiments, an estimate of the temperature in the slipping zone after a slip distance d during the transient can be calculated with the equation (modified from *Carslaw and Jaeger* [1959] as cited by *Di Toro et al.* [2011])

$$T(d) = T_{\mathrm{amb}} + \left\{ \left[\sqrt{v} \left(2\tau_{ss}\sqrt{d} + (\tau_p - \tau_{ss}) \exp\frac{-d}{D_{th}} \sqrt{\pi D_{th}}\,\mathrm{Erf}i\sqrt{\frac{d}{D_{th}}} \right) \right] \cdot \left(2\rho c_p \sqrt{\pi\kappa}\right)^{-1} \right\}, \quad (3)$$

with T_{amb} the ambient temperature. Equation (3) assumes a constant slip rate v and an approximately exponential decay of the shear stress during the transient (i.e., $\tau(d) = \tau_{\mathrm{ss}} + (\tau_{\mathrm{p}} - \tau_{\mathrm{ss}})\exp^{-d/D_{th}}$), as is the case of HVR1388 and HVR1868 (Figures 6a and 7). The thermal weakening dis-

Figure 9. Scanning electron microscope backscattered microphotographs of the experimentally produced Vaiont gouges. Shear sense is left, and high-velocity rotary friction experiments are oriented with the rotational side to the left (Cc = calcite; Qtz = quartz). Room humidity experiments: (a) starting material; (b) HVR1376 at 0.01 m/s; (c) HVR1375 at 0.04 m/s with R-type shears at the contact with the rotational side; (d) HVR1373 at 0.70 m/s with clay clast aggregates (CCA), R- and Y-type shears at the contact with the rotational side; (e) HVR1372 at 1.31 m/s with clay clast aggregates (CCA). Wet experiments: (f) starting material; (g) HTB25 at 0.050 mm/s; (h) HVR1358 at 0.04 m/s; (i) HVR1356 at 0.70 m/s; (j) HVR1388 at 1.31 m/s with P- and Y-type shears.

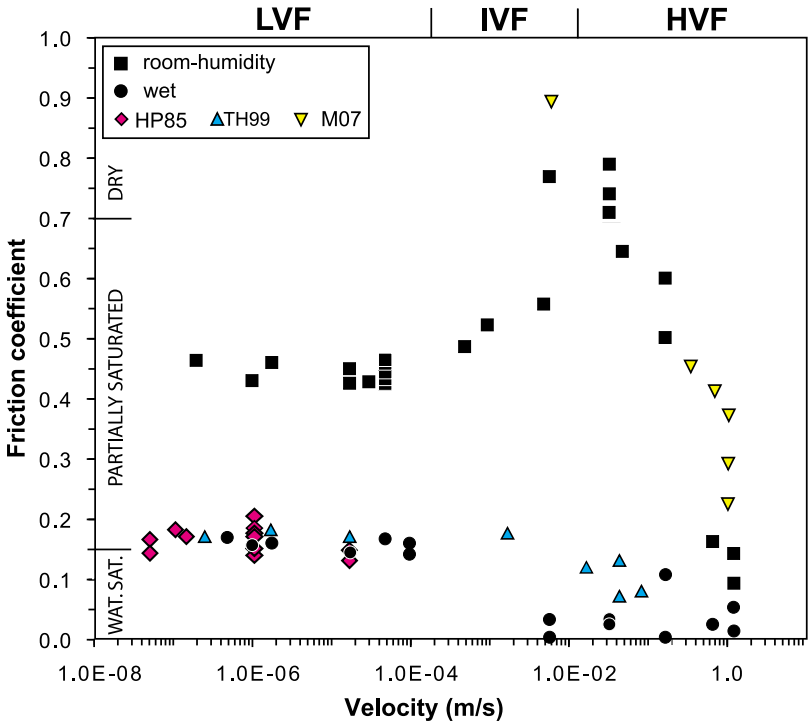

Figure 10. Variation of the steady state friction coefficient as function of velocity in room humidity and wet experiments. LVF = low-velocity friction experiments, IVF = intermediate-velocity friction experiments; HVF = high-velocity friction experiments. Previous results for comparison are HP85 [*Hendron and Patton*, 1985] and TH99 [*Tika and Hutchinson*, 1999] for Vaiont gouges sheared at water-saturated conditions; M07 [*Mizoguchi et al.*, 2007] for Nojima fault gouge, sheared at room humidity conditions. The range of frictional data for montmorillonite-gouges at different fluid content (wat. sat. = water saturated, partially saturated and dry conditions) is from *Moore and Lockner* [2007].

tance D_{th} is defined as the slip distance over which the shear stress decays to a value $\tau_{th} = \tau_{ss} + (1/e)(\tau_p - \tau_{ss})$. ρ, c_p and κ are density (2500 kg/m), thermal capacity at 300 K (900 J/kg/K) and thermal diffusivity (10^{-6} m^2/s) of the clay-rich gouges, respectively. The temperatures calculated according to equation (3) for $d = D_{th}$ in the case of IVF and HVF experiments are (Figure 11)

$$T(d = D_{th}) = T_{amb} + \frac{\sqrt{D_{th} v}\left[2e\tau_{ss} + (\tau_p - \tau_{ss})\sqrt{\pi}\,\mathrm{Erfi}\,1\right]}{2e\rho c_p \sqrt{\pi\kappa}}. \quad (4)$$

At room humidity and ambient temperature of 20°C, the temperature shows no significant variation for slip rates up to 0.70 m/s. Beyond this velocity, the temperature rapidly increases up to about 240°C (Figure 11). This temperature is achieved after ~3 m of slip, which corresponds to the slip distance where the first large dilatancy event is observed in HVR1372, HVR1373 and HVR1868 (see Figure 7 for HVR1372 and HVR1868). Since velocity and frictional heat production are proportional to sample radius, the temperature first increases at the contact between gouge and Teflon® confining ring. *Kitajima et al.* [2010] modeled numerically the temperature distribution in the gouge layer for almost identical experimental conditions (sample geometry, normal stress, slip, slip rate and acceleration). Their model confirms that a temperature increase of 150–200°C is achieved at the edge of the gouge layer between 1 and 5 m of slip and in the center of the gouge layer after ~20 m slip. The progressive increase in temperature toward the inner part of the speci-

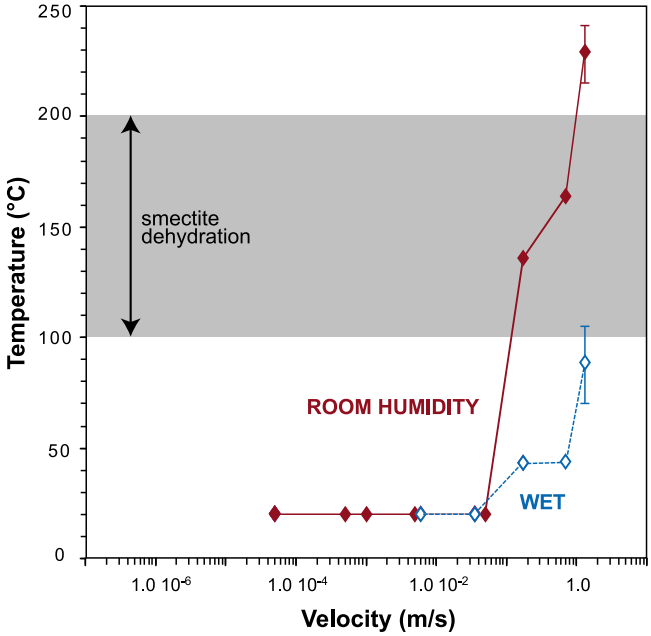

Figure 11. Temperature variation in room humidity and wet experiments as a function of velocity calculated according to equation (3) (see text) of *Di Toro et al.* [2011]. Only during room humidity experiments are the temperatures typical for smectite decomposition (100–200°C [*Bird*, 1984; *Brindley and Brown*, 1980]) achieved.

men might explain the long duration (from 3 to 4 m slip up to ~22 m) of the dilatancy observed in HVR1372 and HVR1868.

[31] Equation (4) slightly overestimates the temperature increase in the slipping zone, as it does not consider the buffering effect of the energy adsorbed during dehydration of smectite and the liquid-vapor transition for water which occurs at ~180°C at 1 MPa [*Lide*, 2008], i.e., almost concomitant with the release of water by smectite. The estimated temperature of 200–250°C calculated with equations (3) and (4) for $v \geq 0.70$ m/s is consistent with the presence of illite-type clays in the slipping zone and Teflon® ring breakdown. In fact, smectite decomposes to illite-type clay in the temperature interval 100–200°C [*Brindley and Brown*, 1980], and the Teflon® breaks down at a temperature of 260°C. The presence of clay clasts aggregates (CCAs) [*Boutareaud et al.*, 2008] only in experiments performed at room humidity conditions and for slip rates of 0.70 and 1.31 m/s supports the hypothesis that deformation occurred above the liquid-vapor phase transition of pore water [*Boutareaud et al.*, 2010]. The CCAs have been interpreted as the result of the combination of the liquid-vapor phase transition of pore water together with the interplay of complex physical and chemical processes [*Boutareaud et al.*, 2010]. However, while the presence of a cortex of clays and utrafine grains wrapping the grain nucleus is evidence for grain rolling, the process of formation of CCAs remains not fully understood and the presence of CCAs it is not evidence by itself of the occurrence of the liquid-vapor transition.

[32] Instead, at wet conditions the estimated (equation (3)) maximum temperature achieved in the slipping zone is limited to 88°C at 1.31 m/s. This temperature is too low to induce smectite decomposition and water release and liquid-vapor transition, and hence, to trigger the conditions which favor the onset of thermal pressurization.

[33] Despite the congruence between the results of the thermal model, the mineral decomposition reactions and the microstructure evolution of the gouge, it must be remembered that the structural and thermal properties (including the activation energy of dehydration reactions) of smectites can be significantly influenced by mechanical deformation so that mineral reactions might take place at lower temperatures with respect to untreated materials [*Dellisanti et al.*, 2006]. It follows that the dehydration of smectite to illite-type clay within the experiments might have occurred at lower temperature.

5.1.2. Room Humidity Experiments

[34] At room humidity conditions and velocity between 0.20 and 100.0 μm/s, the friction coefficient of the clay-rich gouge is 0.43–0.47 (Figure 10) and velocity-weakening/velocity-independent, in agreement with previous experiments performed on smectites under similar ambient conditions (e.g., montmorillonite clay [*Moore and Lockner*, 2007; *Ikari et al.*, 2007]). When velocity increases, the clay-rich gouge is velocity strengthening. The velocity strengthening behavior is observed in the IVF experiments and in the HVF experiments at velocity <0.04 m/s. The friction coefficient increases from 0.43 to maximum 0.71–0.79 at 0.04 m/s. Friction coefficients for clays above ~0.70 have been ascribed to dry conditions (absence of the lubricant effect of moisture), while friction coefficient between 0.15 and 0.70 should result from the amount of water adsorbed on clay surfaces [*Moore and Lockner*, 2007]. Since the strengthening of smectite-rich gouges with decreasing water content is demonstrated in previous experiments [e.g., *Morrow et al.*, 1992; *Ikari et al.*, 2007], the velocity strengthening observed between 0.050 mm/s and 50 mm/s in our experiments could be interpreted as the effect of water removal from the particle surfaces due to frictional heating. However, the temperature estimates (section 5.1.1) indicate that the temperature increment is negligible when the shearing velocity is <0.04 m/s (Figure 11). An alternative way of producing dry contacts among the particles is grain comminution. Comminution, as observed at 0.01 and 0.04 m/s (Figures 9b and 9c), produces new surface of contact among particles which are presumably dry and might increase the gouge friction.

[35] At slip rates >0.04 m/s, the friction coefficient rapidly decreases and the minimum value of 0.09–0.16 is achieved at 0.70 and 1.31 m/s. This dramatic reduction in friction coefficient is similar to that observed by *Mizoguchi et al.* [2007] on the quartz, smectite and kaolinite clay-rich gouges from the Nojima fault and deformed at similar velocity and normal stress (see Figure 10). Though poorly understood, possible weakening mechanisms for the decrease in the friction coefficient above 0.70 m/s are powder lubrication and thermochemical pressurization. Powder lubrication is a not well understood dynamic weakening mechanisms claimed to be active in ultra-fine gouges [*Han et al.*, 2010; *Reches and Lockner*, 2010] and engineering materials (MoS_2, WS_2 [*Higgs et al.*, 1999; *Wornyoh et al.*, 2007]). Thermochemical pressurization is the result of thermal expansion of fluids released, during frictional sliding, by breakdown or decomposition reactions of H_2O or CO_2 bearing minerals [*Brantut et al.*, 2010]. Thermo-chemical pressurization should explain the ~250–280 μm cumulative expansion of the slipping zone observed in HVR1373, HVR1372 (Figure 7a) and HVR1868 (Figure 7b).

[36] As discussed in detail by *Ferri et al.* [2010], in the case of granular flow, the slipping zone might expand with shearing when the chains of grain particles rotate and produce an axial displacement comparable to the length of the grain chains [*Campbell*, 2006]. Although chain rotation is compatible with the thickening of the slipping zone (Figure 7), the rotation would have already occurred several times within the initial 3–4 m displacement and cannot justify the long duration expansion observed from 3.5 to 20–22 m of displacement. Moreover, experiments performed on not-sieved gouges (HVR1372) and gouges sieved at <105 μm (HVR1868) evidenced similar dilatancy despite the different initial grain size.

[37] As discussed above, CCAs should form during grain rolling so their presence in the slipping zone of experiments performed at slip rates above 0.70 m/s supports the occurrence of powder lubrication.. Moreover, in our experiments, for slip rates above 0.70 m/s, the estimated temperature rises to 150–230°C within the first 3 m of displacement. This high temperature is responsible for the decomposition of smectite to an illite-type structure, as demonstrated by the XRPD pattern, with consequent release of water. The amount of water released by smectite collapse at ~200°C depends on the initial hydration [*Bird*, 1984]. *Ferrage et al.* [2007a, 2007b] determined that Ca-montmorillonite dehydration releases 0.06 g of H_2O per gram of montmorillonite

if the initial temperature is 50°C (i.e., the Vaiont clay-rich gouge was kept at 50°C in the oven for 24 h before the experiment). For Vaiont clay-rich gouge (~60% smectite) this water release corresponds to a volume of ~0.04 ml of H_2O per gram of gouge at ambient pressure, although this volume estimate is subject to variability depending on the type of interlayer cations and on the volume of reacted smectite (i.e., not all smectite in the slipping zone decomposes). Unfortunately, the evolution of the gouge volume, porosity and permeability during the experiments cannot be estimated, due to the concomitant occurrences of processes which are poorly constrained (e.g., compaction of the gouge, grain comminution and interaction, formation of boundary layers at the contact with the marble cylinders, dehydration and thinning of smectite, thermal expansion of the gouge material, porosity evolution). However, the development of ultrafine grain layers at the gouge-marble cylinders contacts (Figures 9d and 9e) should keep the permeability low, while the high thermal expansion coefficient of water (thermal expansion of water $\lambda_f = 1.21 \times 10^{-3}$ °C^{-1} [*Rice*, 2006]) and the presence of an almost impermeable Teflon® ring (at least, at the initiation of sliding), should generate significant overpressure. The increment of pressure in the slipping zone is confirmed by the pulsed dilatancy observed in experiments HVR1372and HVR1868 (Figure 7).

[38] A similar evolution of friction coefficient with slip rate (strengthening followed by weakening) was observed in very long slip experiments performed with Westerly Granite under room humidity conditions and similar imposed slip rates and normal stresses [*Reches and Lockner*, 2010]. In this case, the long slip (several hundred of meters) allowed the formation of a ultrafine gouge layer in the slipping zone. Strengthening and weakening are related to gouge produced during sliding which interacted with H_2O from room humidity. In the experiments by *Reches and Lockner* [2010] there are no smectites in the starting material and samples are not confined, thermo-chemical pressurization should be ruled out as a weakening mechanism. Instead, the authors suggested, following *Han et al.* [2010], that weakening resulted from lubrication operated by the presence of micro- to nano-powders. Similarly the large weakening for $v >$ 0.7 m/s in the room humidity experiments reported in Figure 10 could also be the result of thermochemical pressurization (which explains dilatancy) due to smectite decomposition, and powder lubrication due to grain rolling, as attested by the formation of rounded clay-clast aggregates.

5.1.3. Wet Experiments

[39] The 9 October 1963 Vaiont slide occurred under water-saturated conditions and the interpretation of the experiments performed with excess water is relevant to understand the mechanics of the landslide. At a given slip rate, under wet conditions the friction coefficient is 100% (full lubrication) to 70% lower than the friction coefficient under room humidity conditions (Figure 10). The extremely low friction coefficient is the result of a different weakening mechanism from those (thermochemical pressurization and powder lubrication) activated under room humidity conditions, as suggested by the mineralogical and microstructural analysis (Figures 8 and 9). At velocity between 0.20 and 100 μm/s, the friction coefficient is ~0.16 and the reduction of about 70% with respect to the room humidity experiments is consistent with previous experiments performed on dry and wet montmorillonites [*Morrow et al.*, 1992; *Ikari et al.*, 2007]. In this slip rate range, for $\sigma_n \leq$ 5 MPa, the wet Vaiont clay-rich gouges are velocity-weakening (a–b ranging from −0.005 to −0.008). Previous experiments on water saturated smectite-rich gouges evidenced velocity strengthening behavior [e.g., *Morrow et al.*, 1992; *Ikari et al.*, 2009; *Tembe et al.*, 2010] but velocity weakening is also reported [e.g., *Tanikawa and Shimamoto*, 2009]. The transition from velocity strengthening to velocity weakening may depend on the experimental conditions (pressure and velocity range) or composition (amount and type of clay minerals within the gouge) and more systematic investigation is required. When the velocity exceeds 0.01 m/s, friction suddenly decreases to zero. The microstructures remain unaltered up to 0.70 m/s and the grains of calcite and quartz preserve their original size and shape (Figures 9g, 9h, and 9i). Only at v = 1.31 m/s, the gouge develops a deformation structure reported as P- and Y-shears (Figure 9j). The very low friction determines a limited temperature increment during the experiment (<88°C according to equations (3) and (4), see Figure 11), which is inadequate to achieve the decomposition of smectite to illite-type (between 100°C and 200°C [*Brindley and Brown*, 1980; *Bird*, 1984]). We suggest that the onset of full lubrication at $v >$ 0.01 m/s is the result of porosity reduction and progressive expulsion of water. According to this interpretation, sliding occurred on the water layers filling microcracks within the gouge and on a continuous water film formed at the contact between the clay-rich gouge and the marble cylinders.

5.1.4. Comparison With Previous Experiments Performed on Clay-Rich Vaiont Gouges

[40] The role of the Vaiont interbedded clay-rich gouges on the dynamics of the landslide and the influence of the water content on the mechanical properties of the clays was clear since the extensive field work conducted by *Hendron and Patton* [1985]. As a consequence, the frictional properties of the clay-rich gouges from the slide detachment were investigated by several authors [*Hendron and Patton*, 1985; *Tika and Hutchinson*, 1999]. Our locality of sampling corresponds to the same area of provenance of samples 11-3, 11-4 and 11-5 tested by *Hendron and Patton* [1985] and samples 3 and 4 tested by *Tika and Hutchinson* [1999] so that all the experimental results can be compared. This is important, since the mineralogy of the clay-rich gouge layers within the Fonzaso Unit varies along the stratigraphic sequence [*Cobianchi and Picotti*, 2003]. The gouge tested by *Hendron and Patton* [1985] and *Tika and Hutchinson* [1999] was composed of >50% of the clay with the majority of the clay represented by smectite (Ca-montmorillonite [*Hendron and Patton*, 1985]), together with illite, interlayered illite-smectite and large amount of calcite. In Figure 10 we reported for comparison only their experiments performed above 0.5 MPa, since the normal stress affects the friction coefficient [*Saffer and Marone*, 2003]. *Hendron and Patton* [1985] demonstrated that the hydraulic conditions of the Vaiont area were critical and that the movements of the flank of the Toc mountain reflected the variation of rainfall and basin level. For this reason, their experiments were performed only at water-saturated con-

ditions in shear boxes on precut planes, with rates of shearing from 1 to 0.003 mm/min and displacements up to 5 cm. The friction coefficient was 0.13–0.20 and consistent with our LVF experimental data (Figure 10). *Tika and Hutchinson* [1999] investigated a wider velocity range (from 0.24 μm/s to 0.08 m/s) in a ring shear apparatus with displacements up to 3 m. At velocity of 0.24 μm/s, friction was 0.171–0.187 in the presence of excess water and decreased when the imposed slip rate increased (velocity weakening). The reduction of the friction coefficient was proportional to the water content, i.e., 60% reduction at water-saturated conditions (i.e., water maintained within the bath) with $\mu \sim 0.08$, and 17% when water was siphoned out of the bath, corresponding to $\mu \sim 0.15$. The results of *Tika and Hutchinson* [1999] are in agreement with the velocity weakening behavior observed in our wet experiments, though, in the latter, the decrease in friction is more pronounced leading to zero friction (full lubrication). This is probably due to the larger displacements achieved in our experiments.

5.2. Extrapolation to the Vaiont Landslide

[41] Several models [*Vardoulakis*, 2002; *Kilburn and Petley*, 2003; *Helmstetter et al.*, 2004; *Sornette et al.*, 2004; *Veveakis et al.*, 2007; *Pinyol and Alonso*, 2010] explained the mechanism responsible for the frictional evolution of the Vaiont slide by taking into account (1) the data collected from the 2–3 years monitoring preceding the slide collapse [*Mueller*, 1964; *Selli and Trevisan*, 1964] and (2) the experimental results of *Hendron and Patton* [1985] and *Tika and Hutchinson* [1999]. Most models of the mechanics of the Vaiont landslide interpret the field velocity data on the base of several assumptions for the slipping zone (gouge thickness, water content, porosity, permeability and temperature) to infer the evolution of the friction coefficient. It is generally accepted that reservoir (artificial) filling and cumulative rainfall were crucial to trigger slope movements [*Hendron and Patton*, 1985] and that the creep phase of the Vaiont slide was dominated by water-saturated conditions. It is also generally accepted that the high slip rate (estimated to be 20–30 m/s [A*nderson*, 1985]) and large displacement (450 m [*Selli and Trevisan*, 1964]) achieved by the landslide during the final collapse reveal the onset of some dramatic weakening mechanism as thermal pressurization [*Habib*, 1975; *Voight and Faust*, 1982; *Veveakis et al.*, 2007].

[42] Even though our experimental data are not able to solve open questions on Vaiont slide dynamics, as the triggering of the initial movement and the transition from creeping motion to final acceleration, some key remarks can be pointed out regarding the creeping phase and the final collapse.

5.2.1. Creeping Phase of the Slide

[43] During the creeping phase, the condition of stability versus instability of the clay-rich gouges is expressed by the rate and state values of "a" (direct effect) and "b" (evolution effect) [*Helmstetter et al.*, 2004; *Sornette et al.*, 2004]. The difference (a–b) is a material property. From Figure 10 when the gouge is sheared at low slip rates ($v < 0.05$ mm/s), the friction coefficient is ~0.45 under room humidity conditions and ~0.18 under wet conditions.. It follows that the increase in water content drastically reduces the shear strength of the sub-horizontal detachment at the toe of the slide, as observed by *Hendron and Patton* [1985]. In wet conditions, our experiments confirm that the gouge is velocity weakening, i.e., intrinsically unstable as observed by *Tika and Hutchinson* [1999]. This is in agreement with the model proposed by *Helmstetter et al.* [2004] and *Sornette et al.* [2004], who applied to landslide the rate- and state-dependent friction law established in the laboratory to reproduce the movement observed for Vaiont. The alternation of phases of acceleration and deceleration in the period between 1960 and 1963 [*Selli and Trevisan*, 1964; *Hendron and Patton*, 1985] can be explained as the effect of water fluctuations within the clay-rich gouge.

5.2.2. Final Collapse of the Slide

[44] Thermal pressurization is the mechanism most invoked to explain the final velocity of the Vaiont landslide estimated to be 20–30 m/s [*Anderson*, 1985] and triggered by the temperature increase in the slipping zone due to frictional heating during sliding [*Habib*, 1975; *Voight and Faust*, 1982; *Genevois and Ghirotti*, 2005; *Veveakis et al.*, 2007]. However, there are no clear field and experimental studies that show the activation of this weakening mechanism for the Vaiont landslide. This is due to at least three main factors: (1) the slipping zone is below more than 150 m thickness of slide deposits and it is exposed only in the basal detachment along the steep back of the Monte Toc flank, (2) despite the fact that the presence of thin clay layers injected in the bounding limestones beds might suggests some fluidisation and compression of the gouge, the clay-rich gouges do not preserve the microstructures that might have been produced during the dramatic final collapse due to swelling and shrinking of smectite, and (3) there are no friction data from experiments performed at the deformation conditions achieved during the final collapse (slip and slip rates of the order of hundreds of meters and tens of meters per section, respectively).

[45] The estimate of the temperatures achieved during sliding in the slipping zone (equation (4)) implies that only at room humidity conditions and for $v > 0.70$ m/s, can the temperature be higher than 200–300°C. According to our experiments, thermo-chemical pressurization takes place only at room humidity and only at $v > 0.70$ m/s. At wet conditions, which are presumably the conditions during the collapse, deformation localizes along the water films within the gouge layer or at the contact between clay-rich gouge and wall rocks, so the frictional resistance is always very low (full lubrication) and temperature <90°C. As a consequence, at least for $v < 1.31$ m/s, thermal and thermo-chemical pressurization are not required to explain the high slip rates achieved during the final collapse of the landslide.

[46] In this framework, our experimental results do not fit, or only partially support the theoretical models. If such low friction values were achieved in conditions of pure hydrodynamic lubrication, there is no need to invoke for thermal pressurization during the final collapse of the Vaiont landslide and the temperatures in the slipping zone remained below the dehydration temperature for smectite.

6. Conclusions

[47] The 1963 Vaiont slide occurred under water-saturated conditions as effect to intense rainfall and reservoir level. In such case, the hypothesis of thermal and thermo-chemical

pressurization is not required to explain the high velocity achieved by the rock mass during the final collapse, at least for slip rates up to ~1.3 m/s, which is the maximum velocity investigated in this work.

[48] Our experiments performed on the clay-rich gouges from Vaiont basal detachment provide evidence that their frictional properties were controlled by (1) the frictional properties of smectite, (2) the water content of the clays, and (3) the imposed slip rate. Thanks to the very wide velocity range here investigated, it was possible to infer the dynamic evolution of the clay-rich gouges. In particular, at room humidity the friction coefficient is 0.45–0.48 at low velocity and increases to 0.68 at 0.04 m/s (velocity strengthening behavior). At higher slip rates, the friction coefficient decays to 0.09 due to the efficient shear heating which is responsible of a temperature increase up to at least ~260°C. At such high slip rates, the measured dilatancy of the slipping zone, the presence of decomposition products of smectites (i.e., illite type clays) and of Clay Clast Aggregates (CCAs) which might result from grain rolling, support the hypothesis that thermo-chemical pressurization and powder lubrication processes were triggered; at wet conditions, the frictional behavior is always velocity weakening and friction evolves from an initial 0.14–0.18 to almost zero when velocity exceeds 0.01 m/s. In this case, shearing localizes along the water layers among particles or at the clay-rich gouge/wall rock boundary.

[49] **Acknowledgments.** F.F. was supported by CARIPARO (Cassa di Risparmio di Padova e Rovigo) project and G.D.T. by a European Research Council Starting grant 205175 (USEMS). Author contributions are as follows: F.F. and G.D.T. wrote the manuscripts; G.D.T., F.F., T.S. and M.Q. designed the experiments; F.F., T.H., H.N., R.H. and N.D.R. carried out the experiments; F.F. performed the microstructural and mineralogical investigations. G.D.T. thanks David Lockner for enlightening discussions on lubrication in wet clays and Rinaldo Genevois for friendly review of the manuscript. The careful reading and comments by reviewers Diane Moore and Ernie Rutter greatly improved the manuscript.

References

Anderson, D. L. (1985), Calculation of slide velocities, in *The Vaiont Slide, a Geotechnical Analysis Based on New Geologic Observations of the Failure Surface*, edited by A. J. Hendron and F. D. Patton, vol. 2, *Tech. Rep. GL-85-5*, Appendix E and F, U.S. Army Eng. Waterways Exp. Stn., Vicksburg, Miss.

Belloni, L. G., and R. F. Stefani (1992), Natural and induced seismicity at the Vaiont slide, in *Proceedings of the Meeting 1963 Vaiont Landslide*, edited by E. Semenza and G. Melidoro, pp. 115–132, Univ. of Ferrara, Ferrara, Italy.

Bird, P. (1984), Hydration-phase diagrams and friction of montmorillonite under laboratory and geologic conditions, with implications for shale compaction, slope stability, and strength of fault gouge, *Tectonophysics*, *107*, 235–260, doi:10.1016/0040-1951(84)90253-1.

Boutareaud, S., D. G. Calugaru, R. Han, O. Fabbri, K. Mizoguchi, A. Tsutsumi, and T. Shimamoto (2008), Clay-clasts aggregates: A new textural evidence for seismic fault sliding?, *Geophys. Res. Lett.*, *35*, L05302, doi:10.1029/2007GL032554.

Boutareaud, S., A. M. Boullier, M. André, D. G. Calugaru, P. Beck, S. R. Song, and T. Shimamoto (2010), Clay clast aggregates in gouges: New textural evidence for seismic faulting, *J. Geophys. Res.*, *115*, B02408, doi:10.1029/2008JB006254.

Brantut, N., A. Schubnel, J. Corvisier, and J. Sarout (2010), Thermochemical pressurization of faults during coseismic slip, *J. Geophys. Res.*, *115*, B05314, doi:10.1029/2009JB006533.

Brindley, G. W., and G. Brown (1980), *Crystal Structure of Clay Minerals and Their X-Ray Identification*, *Mineral. Soc. Monogr.*, vol. 5, 495 pp., Mineral. Soc., London.

Campbell, C. (2006), Granular material flows–an overview, *Powder Technol.*, *162*, 208–229, doi:10.1016/j.powtec.2005.12.008.

Carslaw, H. S., and J. C. Jaeger (1959), *Conduction of Heat in Solids*, 510 pp., Clarendon Press, Oxford, U. K.

Chester, F. M., and J. S. Chester (1998), Ultracataclasite structure and friction processes of the Punchbowl Fault, San Andreas System, California, *Tectonophysics*, *295*, 199–221, doi:10.1016/S0040-1951(98)00121-8.

Cobianchi, M., and V. Picotti (2003), The Vaiont gorge section: The Toarcian to Bajocian Igne Formation and the unconformable base of the Vaiont Limestone, in *General Field Trip Guidebook, 6th International Symposium on the Jurassic System, 12–22 September 2002, Palermo, Italy*, edited by M. Santantonio, pp. 310–312, Litografia GEDA, Turin, Italy.

Cocco, M., E. Tinti, C. Marone, and A. Piatanesi (2009), Scaling of slip weakening distance with final slip during dynamic earthquake rupture, in *Fault-Zone Properties and Earthquake Rupture Dynamics*, *Int. Geophys. Ser.*, vol. 94, edited by E. Fukuyama, pp. 163–186, Academic, Burlington, Mass.

Dellisanti, F., V. Minguzzi, and G. Valdrè (2006), Thermal and structural properties of Ca-rich Montmorillonite mechanically deformed by compaction and shear, *Appl. Clay Sci.*, *31*, 282–289, doi:10.1016/j.clay.2005.09.006.

Di Toro, G., R. Han, T. Hirose, N. De Paola, S. Nielsen, K. Mizoguchi, F. Ferri, M. Cocco, and T. Shimamoto (2011), Fault lubrication during earthquakes, *Nature*, *471*, 494–498, doi:10.1038/nature09838.

Dieterich, J. H. (1979), Modeling of rock friction: 1. Experimental results and constitutive Equations, *J. Geophys. Res.*, *84*, 2161–2168, doi:10.1029/JB084iB05p02161.

Faulkner, D. R., A. C. Lewis, and E. H. Rutter (2003), On the internal structure and mechanics of large strike-slip fault zones; field observations of the Carboneras Fault in southeastern Spain, *Tectonophysics*, *367*, 235–251, doi:10.1016/S0040-1951(03)00134-3.

Ferrage, E., C. A. Kirk, G. Cressey, and J. Cuadros (2007a), Dehydration of Ca montmorillonite at the crystal scale. Part 1: Structure evolution, *Am. Mineral.*, *92*, 994–1006, doi:10.2138/am.2007.2396.

Ferrage, E., C. A. Kirk, G. Cressey, and J. Cuadros (2007b), Dehydration of Ca-montmorillonite at the crystal scale. Part 2: Mechanisms and kinetics, *Am. Mineral.*, *92*, 1007–1017, doi:10.2138/am.2007.2397.

Ferri, F., G. Di Toro, T. Hirose, and T. Shimamoto (2010), Evidences of thermal pressurization in high velocity friction experiments on smectite-rich gouges, *Terra Nova*, *22*, 347–353, doi:10.1111/j.1365-3121.2010.00955.x.

Genevois, R., and M. Ghirotti (2005), The 1963 Vaiont landslide, *G. Geol. Appl.*, *1*, 41–53.

Habib, P. (1967), Sur un mode de glissement des massifs rocheaux, *C. R. Seances Acad. Sci.*, *264*, 151–153.

Habib, P. (1975), Production of gaseous pore pressure during rock slides, *Rock Mech.*, *7*, 193–197, doi:10.1007/BF01246865.

Han, R., T. Hirose, and T. Shimamoto (2010), Strong velocity weakening and powder lubrication of simulated carbonate faults at seismic slip rates, *J. Geophys. Res.*, *115*, B03412, doi:10.1029/2008JB006136.

Helmstetter, A., D. Sornette, J.-R. Grasso, J. V. Andersen, S. Gluzman, and V. Pisarenko (2004), Slider block friction model for landslides: Application to Vaiont and La Clapière landslides, *J. Geophys. Res.*, *109*, B02409, doi:10.1029/2002JB002160.

Hendron, A. J., and F. D. Patton (1985), *The Vaiont Slide, A Geotechnical Analysis Based on New Geologic Observations of the Failure Surface*, *Tech. Rep. GL-85-5*, U.S. Army Corps of Eng., Washington, D. C.

Hendron, A. J., and F. D. Patton (1987), The Vaiont slide–A geotechnical analysis based on new geological observations of the failure surface, *Eng. Geol. Amsterdam*, *24*, 475–491, doi:10.1016/0013-7952(87)90080-9.

Hickman, S., M. Zoback, and W. Ellsworth (2005), Structure and composition of the San Andreas Fault Zone at Parkfield: Results from SAFOD Phase 1 and 2, *Eos Trans AGU*, *87*(52), Fall Meet. Suppl., Abstract T23E-05.

Higgs, F. C., C. A. Heshmat, and H. Heshmat (1999), Comparative evaluation of MoS2 and WS2 as powder lubricants in high speed, multi pad journal bearing, *J. Tribol.*, *121*, 625–630, doi:10.1115/1.2834113.

Hirose, T., and T. Shimamoto (2005), Growth of molten zone as a mechanism of slip weakening of simulated faults in gabbro during frictional melting, *J. Geophys. Res.*, *110*, B05202, doi:10.1029/2004JB003207.

Ikari, M. J., D. M. Saffer, and C. Marone (2007), Effect of hydration state on the frictional properties of montmorillonite-based fault gouge, *J. Geophys. Res.*, *112*, B06423, doi:10.1029/2006JB004748.

Ikari, M. J., D. M. Saffer, and C. Marone (2009), Frictional and hydrologic properties of clay-rich fault gouge, *J. Geophys. Res.*, *114*, B05409, doi:10.1029/2008JB006089.

Kilburn, C. R. J., and D. N. Petley (2003), Forecasting giant, catastrophic slope collapse: Lessons from Vaiont, northern Italy, *Geomorphology*, *54*, 21–32, doi:10.1016/S0169-555X(03)00052-7.

Kitajima, H., J. S. Chester, F. M. Chester, and T. Shimamoto (2010), High-speed friction of disaggregated ultracataclasite in rotary shear: Characterization of frictional heating, mechanical behavior, and microstructure evolution, *J. Geophys. Res.*, *115*, B08408, doi:10.1029/2009JB007038.

Lide, D. R. (2008), *CRC Handbook of Chemistry and Physics*, 89th ed., edited by D. R. Lide, CRC Press, Boca Raton, Fla.

Makinson, K. R., and D. Tabor (1964), The friction and transfer of PTFE, *Proc. R. Soc. London*, *281*, 49–61, doi:10.1098/rspa.1964.0168.

Marone, C. (1998), Laboratory-derived friction laws and their application to seismic faulting, *Annu. Rev. Earth Planet. Sci.*, *26*, 643–696, doi:10.1146/annurev.earth.26.1.643.

Mizoguchi, K., T. Hirose, T. Shimamoto, and E. Fukuyama (2007), Reconstruction of seismic faulting by high-velocity friction experiments: An example of the 1995 Kobe earthquake, *Geophys. Res. Lett.*, *34*, L01308, doi:10.1029/2006GL027931.

Mizoguchi, K., T. Hirose, T. Shimamoto, and E. Fukuyama (2009), High-velocity frictional behavior and microstructure evolution of fault gouge obtained from Nojima fault, southwest Japan, *Tectonophysics*, *471*, 285–296, doi:10.1016/j.tecto.2009.02.033.

Moore, D. E., and D. A. Lockner (2007), Friction of the smectite clay montmorillonite: A review and interpretation of data, in *The Seismogenic Zone of Subduction Thrust Faults*, *MARGINS Theoret. d Exp. Earth Sci. Ser.*, vol. 2, edited by T. H. Dixon and C. Moore, pp. 317–345, Columbia Univ. Press, New York.

Morrow, C. A., B. Radney, and J. D. Byerlee (1992), Frictional strength and the effective pressure law of montmorillonite and illite clays, in *Fault Mechanics and Transport Properties of Rocks*, edited by B. Evans and T. F. Wong, pp. 69–88, Academic, San Diego, Calif., doi:10.1016/S0074-6142(08)62815-6.

Mueller, L. (1964), The rock slide in the Vaiont Valley, *Rock Mech. Eng. Geol.*, *2*, 148–212.

Niemeijer, A. R., and C. J. Spiers (2006), Velocity dependence of strength and healing behaviour in simulated phyllosilicate-bearing fault gouge, *Tectonophysics*, *427*, 231–253, doi:10.1016/j.tecto.2006.03.048.

Noda, H., and T. Shimamoto (2009), Constitutive properties of clayey fault gouge from the Hanaore fault zone, southwest Japan, *J. Geophys. Res.*, *114*, B04409, doi:10.1029/2008JB005683.

Pinyol, N. M., and E. E. Alonso (2010), Criteria for rapid sliding II. Thermo-hydro-mechanical and scale effects in Vaiont case, *Eng. Geol.*, *114*, 211–227, doi:10.1016/j.enggeo.2010.04.017.

Reches, Z., and D. A. Lockner (2010), Fault weakening and earthquake instability by powder lubrication, *Nature*, *467*, 452–455, doi:10.1038/nature09348.

Rice, J. R. (2006), Heating and weakening of faults during earthquake slip, *J. Geophys. Res.*, *111*, B05311, doi:10.1029/2005JB004006.

Ruina, A. L. (1983), Slip instability and state variable friction laws, *J. Geophys. Res.*, *88*, 10,359–10,370, doi:10.1029/JB088iB12p10359.

Saffer, D. M., and C. Marone (2003), Comparison of smectite- and illite-rich gouge frictional properties: Application to the updip limit of the seismogenic zone along subduction megathrusts, *Earth Planet. Sci. Lett.*, *215*, 219–235, doi:10.1016/S0012-821X(03)00424-2.

Schleicher, A. M., L. N. Warr, and B. A. van der Pluijm (2009), On the origin of mixed-layered clay minerals from the San Andreas Fault at 2.5–3 km vertical depth (SAFOD drillhole at Parkfield, California), *Contrib. Mineral. Petrol.*, *157*, 173–187, doi:10.1007/s00410-008-0328-7.

Selli, R., and L. Trevisan (1964), Caratteri e interpretazione della frana del Vaiont, *G. Geol.*, *32*, 7–103.

Semenza, E. (1965), Sintesi degli studi geologici sulla frana del Vaiont dal 1959 al 1964, *Mem. Mus. Tridentino Sci. Nat.*, *16*, 1–52.

Semenza, E., and M. Ghirotti (2000), History of 1963 Vaiont Slide. The importance of the geological factors to recognise the ancient landslide, *Bull. Eng. Geol. Environ.*, *59*, 87–97, doi:10.1007/s100640000067.

Shimamoto, T., and A. Tsutsumi (1994), A new rotary-shear high velocity frictional testing machine: Its basic design and scope of research (in Japanese with English abstract), *Struct. Geol.*, *39*, 65–78.

Sornette, D., A. Helmstetter, J. V. Adersen, S. Gluzman, J. R. Grasso, and V. Pisarenko (2004), Towards landslide predictions: Two case studies, *Physica A*, *338*, 605–632, doi:10.1016/j.physa.2004.02.065.

Tanikawa, W., and T. Shimamoto (2009), Frictional and transport properties of the Chelungpu fault from shallow borehole data and their correlation with seismic behavior during the 1999 Chi-Chi earthquake, *J. Geophys. Res.*, *114*, B01402, doi:10.1029/2008JB005750.

Tembe, S., D. A. Lockner, and T. F. Wong (2010), Effect of clay content and mineralogy on frictional sliding behavior of simulated gouges: Binary and ternary mixtures of quartz, illite and montmorillonite, *J. Geophys. Res.*, *115*, B03416, doi:10.1029/2009JB006383.

Tika, T. E., and J. N. Hutchinson (1999), Ring shear tests on soil from the Vaiont landslide slip surface, *Geotechnique*, *49*, 59–74, doi:10.1680/geot.1999.49.1.59.

Vardoulakis, I. (2002), Dynamic thermo-poro-mechanical analysis of catastrophic landslides, *Geotechnique*, *52*, 157–171, doi:10.1680/geot.2002.52.3.157.

Veveakis, E., I. Vardoulakis, and G. Di Toro (2007), Thermoporomechanics of creeping landslides: The 1963 Vaiont slide, northern Italy, *J. Geophys. Res.*, *112*, F03026, doi:10.1029/2006JF000702.

Voight, B., and C. Faust (1982), Frictional heat and strength loss in some rapid landslides, *Geotechnique*, *32*, 43–54, doi:10.1680/geot.1982.32.1.43.

Wornyoh, E. Y. A., V. K. Jasti, and C. F. Higgs (2007), A review of dry particulate lubrication: Powder and granular materials, *J. Tribol.*, *129*, 438–449, doi:10.1115/1.2647859.

N. de Rossi and M. Quaresimin, Dipartimento di Ingegneria dei Sistemi Industriali, Università degli Studi di Padova, Stradella S. Nicola, 3, I-36100 Vicenza, Italy.

G. Di Toro and F. Ferri, Dipartimento di Geoscienze, University of Padova, via G. Gradenigo, 6, I-35131 Padova, Italy. (fabio.ferri@unipd.it)

R. Han, Korea Institute of Geoscience and Mineral Resources, 92 Gwahang-no Yuseong-gu, Daejeon 305-350, South Korea.

T. Hirose, Kochi Institute for Core Sample Research, JAMSTEC, Nankoku, Kochi 783-8502, Japan.

H. Noda, Seismological Laboratory, California Institute of Technology, 1200 E. California Blvd., MS 252-21, Pasadena, CA 91125, USA.

T. Shimamoto, State Key Laboratory of Earthquake Dynamics, Institute of Geology, Chinese Earthquake Administration, PO Box 9803, Beijing 100029, China.